

Metallicity Dependence of Giant Planets around M Dwarfs

TIANJUN GAN ¹, CHRISTOPHER A. THEISSEN ², SHARON X. WANG ¹, ADAM J. BURGASSER ², AND SHUDE MAO ¹

¹*Department of Astronomy, Tsinghua University, Beijing 100084, People's Republic of China*

²*Center for Astrophysics and Space Sciences, University of California, San Diego, 9500 Gilman Dr, La Jolla, CA 92093, USA*

ABSTRACT

We investigate the stellar metallicity ([Fe/H] and [M/H]) dependence of giant planets around M dwarfs by comparing the metallicity distribution of 746 field M dwarfs without known giant planets with a sample of 22 M dwarfs hosting confirmed giant planets. All metallicity measurements are homogeneously obtained through the same methodology based on the near-infrared spectra collected with a single instrument SpeX mounted on the NASA Infrared Telescope Facility. We find that 1) giant planets favor metal-rich M dwarfs at a 4-5 σ confidence level, depending on the band of spectra used to derive metallicity; 2) hot ($a/R_* \leq 20$) and warm ($a/R_* > 20$) Jupiters do not show a significant difference in the metallicity distribution. Our results suggest that giant planets around M and FGK stars, which are already known to prefer metal-rich hosts, probably have a similar formation channel. In particular, hot and warm Jupiters around M dwarfs may have the same origin as they have indistinguishable metallicity distributions. With the refined stellar and planetary parameters, we examine the stellar metallicities and the masses of giant planets where we find no significant correlation. M dwarfs with multiple giant planets or with a single giant planet have similar stellar metallicities. Mid-to-late type M stars hosting gas giants do not show an apparent preference to higher metallicities compared with those early-M dwarfs with gas giants and field M dwarfs.

Keywords: M dwarfs; Giant planets; Stellar properties; Stellar metallicity; Spectroscopy; Astrostatistics

1. INTRODUCTION

Since the first detection of a hot Jupiter around a solar-type star outside the Solar System (Mayor & Queloz 1995), the formation channel of giant planets has been under debate over the last two decades. One of the leading hypotheses is core accretion (e.g., Pollack et al. 1996; Ida & Lin 2004a; Mordasini et al. 2008), a bottom-up mechanism starting with a massive solid core that eventually grows into a giant planet through runaway gas accretion before the disk dissipates.

Several pieces of observational evidence have been put forward in support of such a scenario. For example, metal-rich stars appear to be more likely to host cold giant planets found by radial velocity (RV) surveys (e.g., Gonzalez 1997; Santos et al. 2004; Fischer & Valenti 2005; Johnson et al. 2010; Montet et al. 2014; Adibekyan

2019), the so-called giant planet-metallicity correlation. Under the core accretion paradigm, as the bulk metallicity is supposed to reflect the amount of materials available in the protoplanetary disk, one would naturally expect that gas giants form more easily around stars with higher metallicity. Maldonado et al. (2012) went a step further and compared the stellar metallicity preference of hot and cool Jupiter systems, where the authors pointed out a lower frequency of hot Jupiters than cool ones at low metallicities. Later work from Petigura et al. (2018) looked into the metallicity dependence of planet occurrence rate with a sample of *Kepler* targets (Borucki et al. 2010) and reported a steeper trend towards short-period gas giants. With a larger sample, Narang et al. (2018) studied the average metallicity of stars with planets in two period bins split at 10 days. Although stars with short-period small planets ($M_p \leq 50 M_\oplus$) tend to be more metal-rich than those hosting longer period ones, such a trend is not significant when moving to the giant planet branch, which further complicates the picture. More recently, Osborn & Bayliss (2020) revis-

ited the planet–metallicity correlation for hot Jupiters by comparing the metallicity distribution of hot Jupiter hosts and that of a field star population simulated using the Besançon Galaxy model (Robin et al. 2003). They confirmed that hot Jupiters prefer metal-rich stars but the correlation coefficient is roughly comparable with gas giant planets with longer periods, indicating a similar formation origin.

However, most aforementioned efforts were made to FGK stars, equivalent relevant studies on giant planets around M dwarfs are still lacking so far even though M stars are the dominant stellar population in the solar neighborhood (Henry et al. 2006; Reylé et al. 2021). This is not only because of the difficulty in determining the M dwarf stellar properties but also due to the low occurrence rate of both hot and cold Jupiters around M dwarfs in contrast to other types of stars. Gan et al. (2023a) found a frequency of $0.27 \pm 0.09\%$ for hot Jupiters around early-type M dwarfs and the number slightly decreases to $0.137 \pm 0.097\%$ around late-type M stars (Bryant et al. 2023; Pass et al. 2023). Regarding cold Jupiters, Johnson et al. (2010) estimated 0.03 ± 0.02 giant planets per M star within 2.5 AU (see also Sabotta et al. 2021). Nevertheless, a few such high-mass-ratio systems (e.g., Morales et al. 2019; Gan et al. 2023b; Hartman et al. 2024; Bryant et al. 2024; Stefansson et al. 2024; Hotnisky et al. 2024) were found to stretch the core accretion theory and may favor the gravitational instability model (Boss 2002) instead, making them particularly crucial to understand the giant planet formation. Plenty of techniques such as broadband photometry-based empirical relations (e.g., Terrien et al. 2012; Mann et al. 2013, 2015, 2019; Newton et al. 2014, 2015) and detailed spectroscopic analysis (e.g., Veyette et al. 2016; Marfil et al. 2021; Passegger et al. 2022; Bello-García et al. 2023; Jahandar et al. 2024) have been developed to determine the stellar parameters of M dwarfs, allowing for better characterizations for M dwarf planetary systems (Gore et al. 2024).

Based on photometric calibrations, early work from Johnson & Apps (2009) found that M dwarfs with planets tend to have metallicities in excess of field M stars in the solar neighborhood. Rojas-Ayala et al. (2010) later reported that M dwarfs hosting Jovian-like planets detected by RV surveys have higher metallicities than those with Neptune- or Earth-size planets but the sample size is limited. Using a sample of three M dwarfs with RV-detected giant planets, Gaidos & Mann (2014) found that they are not significantly more metal-rich than the average parent sample and the power-law index relating planet occurrence rate to stellar metallicity is consistent with Sun-like star counterparts within uncertain-

ties. In terms of hot Jupiters, the Transiting Exoplanet Survey Satellite (TESS; Ricker et al. 2015) has been enlarging the number, where most of them were detected around high-metallicity M stars (e.g., Gan et al. 2022; Kanodia et al. 2022; Kageyama et al. 2023; Han et al. 2024). In addition, Gan et al. (2023b) claimed a possible trend that hot Jupiters prefer more metal-rich M stars than warm Jupiters based on the literature metallicity measurements but the heterogeneous instruments and methodologies result in systematic biases, preventing a firm conclusion.

In this manuscript, we compare the metallicity ($[\text{Fe}/\text{H}]$ and $[\text{M}/\text{H}]$) distributions of 22 M dwarfs hosting confirmed giant planets (defined as planets with mass $0.2 M_{\text{Jup}} \leq M_p < 13.6 M_{\text{Jup}}$) with a field M dwarf sample and investigate the difference between the hot and warm Jupiter groups. All metallicities are homogeneously measured using the near-infrared low-resolution spectra from a single instrument SpeX (Rayner et al. 2003) mounted on the 3.2-m NASA Infrared Telescope Facility (IRTF), through the same method. Compared with previous works (Johnson & Apps 2009; Rojas-Ayala et al. 2010; Gaidos et al. 2014), our giant planet sample is about four times larger and includes several short-period gas giants detected by the TESS mission, which allows us to separate our sample into hot and warm Jupiters and study the metallicity preference of these two sub-groups. We refine the stellar and planet properties of our planet sample and explore potential correlations with stellar metallicity. The rest of the paper is structured as follows. We begin with sample construction in Section 2. We summarize our SpeX observations in Section 3. Section 4 describes how we determine the metallicity and refine the stellar and planet parameters. In Section 5, we conduct the metallicity comparison between two samples. We conclude our findings in Section 6.

2. SAMPLE CONSTRUCTION

2.1. Field M Dwarf Sample

The field M dwarf sample is constructed based on the SpeX spectroscopic survey carried out by Terrien et al. (2012) between 2011 and 2013. The whole stellar sample consisted of 886 nearby M dwarfs mostly selected according to their proper motions (Lépine & Shara 2005; Lépine & Gaidos 2011) with a small set of planet hosts as well as wide binaries that serve as abundance calibration stars (Rojas-Ayala et al. 2010). All targets were observed with SpeX in the short cross-dispersed (SXD) mode at a spectral resolving power of ≈ 2000 covering the *JHK* bands simultaneously. Later work from Terrien et al. (2015) provided the $[\text{Fe}/\text{H}]$ and $[\text{M}/\text{H}]$ mea-

measurements for most stars based on different calibrations (see Section 4). We refer the readers to Terrien et al. (2015) for more details about the survey description, observations, and data reduction.

To obtain precise stellar properties, we crossmatch the full catalog with Gaia DR3 (Gaia Collaboration et al. 2023) through their 2MASS identifiers (Cutri et al. 2003; Skrutskie et al. 2006) to retrieve the stellar kinematic properties. We restrict the sample to stars with parallax and proper motion measurements from Gaia, which excluded 109 stars. We do not make a specific cut on the significance of these measurements as most stars are nearby and have well-determined parallax and proper motions. We find that 24 stars in Terrien et al. (2015) do not have metallicity measurements, thus we remove them from our sample. To minimize the effect of giant planets in the field M dwarf sample, we filter out and exclude 7 known giant planet M dwarf hosts, all of which are included in our planet sample below, thus the final field M star sample ends with 746 stars. The full catalog is available in Table 1. We note that we do not have prior information on whether the rest of the stars in the field M dwarf sample host giant planets since most of them do not have radial velocity follow-up observations. Therefore, the field M dwarf group could be regarded as a mixed sample, containing stars without gas giants as well as a small fraction of stars hosting giant planets. Here, we demonstrate that such a contamination will not affect the final conclusion. According to the occurrence rate measurements, we conservatively estimate that there are about two M dwarfs hosting hot Jupiters and twenty M stars harboring cold Jupiters in the field M dwarf sample (Sabotta et al. 2021; Gan et al. 2023a; Bryant et al. 2023). We randomly choose 22 stars in the field M dwarf sample, assuming they host giant planets and have the highest metallicity (0.7 dex) as in our planet sample. We repeat the simulation above for 5000 times and we find the metallicity distribution almost does not change with the median [Fe/H] varying between -0.07 and -0.06 dex for the *H*-band measurements, 0.07 and 0.08 dex for the *K*-band measurements as well as [M/H] ranging between -0.04 and -0.02 dex for the *H*-band results, 0.0 and 0.02 dex for the *K*-band results, all of which are within 1σ .

2.2. M Dwarf Giant Planet Sample

We constructed the M dwarf giant planet sample with the help of information from the NASA Exoplanet Archive (Akeson et al. 2013) accessed on 2023 April 1st. We accepted all M dwarfs with effective temperature $T_{\text{eff}} < 4000$ K and stellar mass $M_* < 0.65 M_{\odot}$ that have confirmed giant planets with mass $0.2 M_{\text{Jup}} \leq M_p <$

$13.6 M_{\text{Jup}}$ detected by either transit or radial velocity surveys. The raw selection during this step is based on stellar parameters from the literature, thus from different sources (i.e., spectroscopic facilities and methodologies). Both stellar and planet parameters are refined in a homogeneous way (see Section 4). After excluding objects that are beyond the sky coverage of SpeX ($\text{Dec} < -30^\circ$), a total of 22 M dwarfs including 5 multi-giant-planet systems (GJ 1148, GJ 317, GJ 3512, GJ 849 and GJ 876) are left. Figure 1 shows the color-magnitude diagram and the refined stellar mass versus effective temperature distribution of the two samples. Our planet sample eventually contains these 22 M stars with 27 giant planets.

We emphasize that our planet sample includes planetary systems detected by different surveys, and the potential bias between different selection functions is challenging to characterize. Therefore, we are not able to probe the giant planet occurrence rates in different stellar metallicity bins as other works (e.g., Fischer & Valenti 2005). Instead, we treat the M dwarf planet sample and the field M dwarf group as independent populations and test whether their metallicities could be drawn from a single distribution. The reason is that M dwarfs with confirmed giant planets are rare. For a specific transit or RV survey, the total number of detected systems is limited, prohibiting attempts to compare the occurrence rates in several metallicity bins due to large Poisson noise.

3. SPEX OBSERVATIONS

We collected at least two ABBA nod sequences (8 exposures) for every giant planet host star¹ in our planet sample on 2023 August 9th and 11th, and December 28th using SpeX with the same observation configuration as Terrien et al. (2012), under the program 2023B078. We applied the short cross-dispersed (SXD) mode with the $0''.3 \times 15''$ slit aligned with the parallactic angle at a spectral resolving power of ≈ 2000 , spanning a wavelength range of 0.8–2.4 μm . After the target observation, we obtained the spectrum of a nearby standard A0 star at an equivalent airmass for flux and telluric calibrations, followed by arc lamp and flat field lamp exposures. All spectroscopic data were then reduced using SpeXtool v4.1 (Cushing et al. 2004) using standard settings and shifted to the rest frame. The resulting merged spectra have a signal-to-noise ratio (SNR) $\gtrsim 100$, all of which are shown in Figure 2.

¹ The SpeX spectra of three targets NGTS-1, TOI-519 and TOI-530 were retrieved from Gore et al. (2024), which were taken using the same mode as here and Terrien et al. (2012).

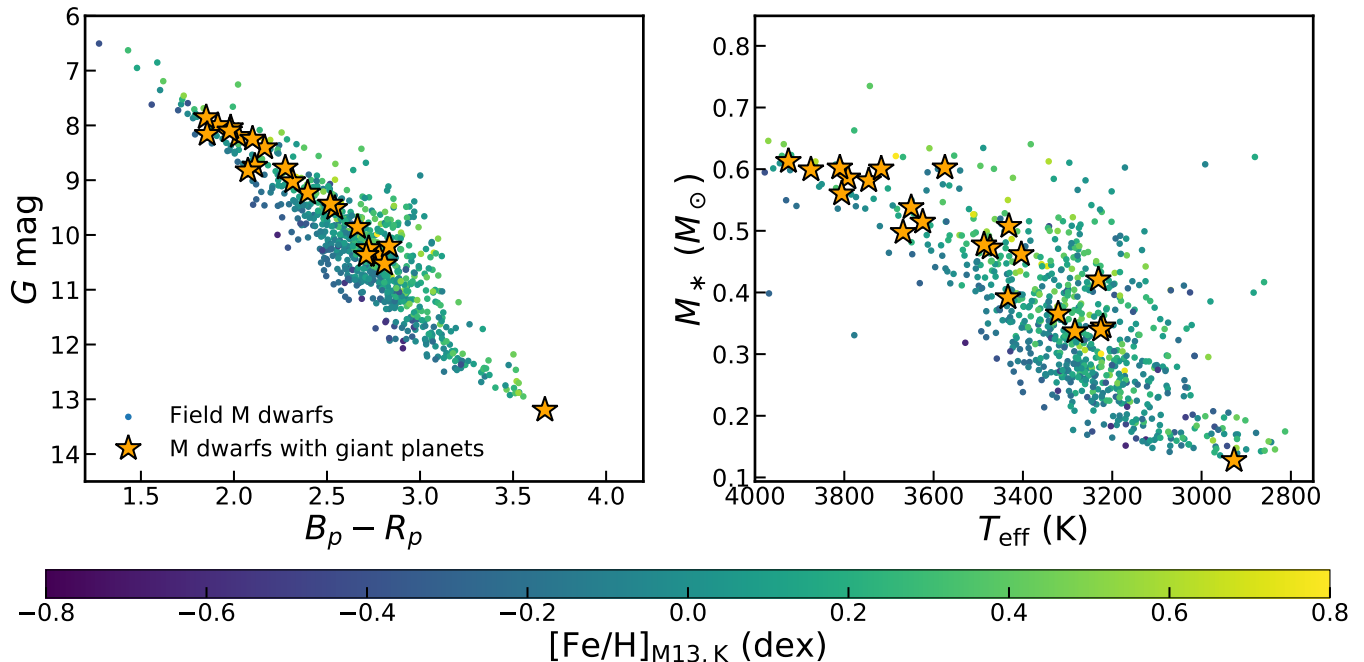


Figure 1. *Left panel:* The Gaia color–magnitude diagram of 746 field M dwarfs colored by their $[\text{Fe}/\text{H}]$, and 22 M stars with confirmed giant planets marked as orange stars. *Right panel:* The refined stellar masses and effective temperatures of two samples (see Section 4 for details).

4. ANALYSIS

4.1. Metallicity

We first determined the spectral types for the planet sample by comparing the 1d merged spectra to the IRTF spectral library (Cushing et al. 2005; Rayner et al. 2009). We utilized the SPLAT code (Burgasser & Splat Development Team 2017) to normalize the data and find the best matches through χ^2 minimization. In the match, we exclude the regions close to 1.1–1.2, 1.3–1.5 and 1.75–2.0 μm with strong telluric absorption that may dominate the residuals. We show an example of our spectrum match in Figure 3.

The spectral types of the field M dwarf sample come from Terrien et al. (2015), which instead applied the NIR calibration developed in Newton et al. (2014) based on the $\text{H}_2\text{O-K2}$ index defined by Rojas-Ayala et al. (2012). We examined the consistency of spectral type (SpT) between two methods with the 7 overlapped giant planet host stars and we find that $\Delta_{\text{SpT}} \leq 1.0$. We thus neglected the difference and used them as inputs from the same source in the following steps. The spectral type of our planet sample ranges from M0V to M5V while the field M dwarf sample spans M0V to M5.5V.

Building on the derived spectral types, we measured the iron abundance $[\text{Fe}/\text{H}]$ and overall metallicity $[\text{M}/\text{H}]$ following the same method as in Terrien et al. (2015). We made use of the `metal` algorithm (Mann et al. 2013) to determine the metallicity based on the H -band (Ter-

rien et al. 2012) and K -band (Rojas-Ayala et al. 2012) relations. The methodology is calibrated with a sample of wide binaries containing a Sun-like primary and a low-mass M star secondary, by determining the correlation between the metallicity of the central star and the features in the companion dwarf spectra (Mann et al. 2013). Since the J -band calibration has a larger scatter, we chose not to use it in this work. We note that the K -band spectra are expected to provide more accurate metallicity results because they are less affected by the telluric contamination than H -band spectra (Dressing et al. 2019). The systematic errors of H - and K -band calibrations are 0.09 and 0.08 dex, which are considered in the following analysis.

Figure 4 presents the comparisons of $[\text{Fe}/\text{H}]$ and $[\text{M}/\text{H}]$ outputs from H and K band spectra with subscripts of $M13,H$ and $M13,K$. Overall, we find that the results agree well with each other although the K -band outputs appear to be slightly higher than those from H -band toward the high metallicity end. The discrepancy might be due to the wavelength calibration or the data reduction procedure but the exact reason for the offset is still unclear. Therefore, we chose to independently investigate the metallicity distribution based on the results from two bands. We caution the readers these calibrations were untested for M dwarfs beyond M5 and metallicity greater than 0.56 dex and the corresponding outputs could be interpreted as extrapolations since the

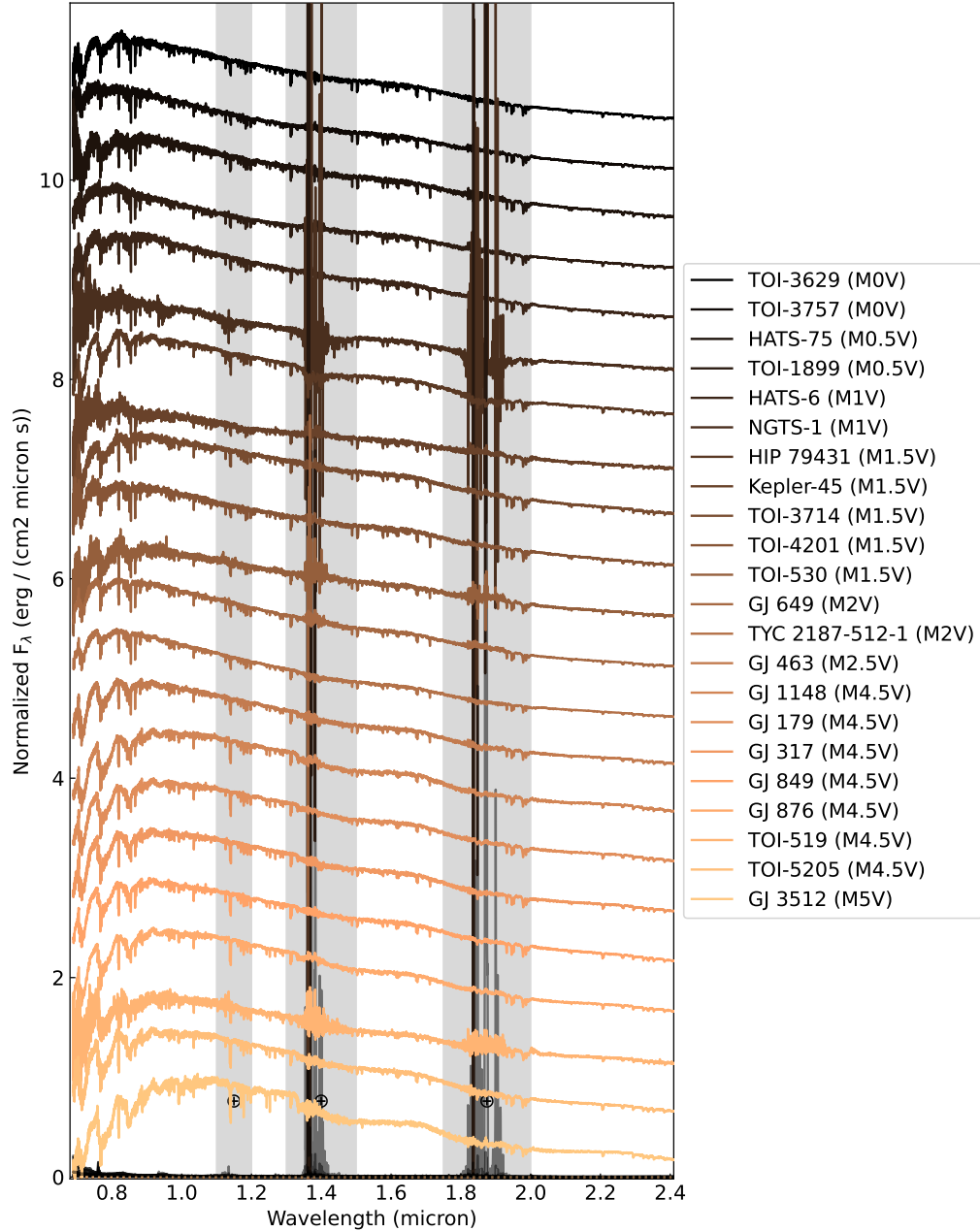


Figure 2. The normalized SpeX spectra of 22 M dwarfs with confirmed giant planets. The data are presented in the order of stellar types derived through spectrum match (see Section 4). Three vertical grey areas mark telluric absorption features, which we excluded during the analysis. All SpeX spectra we collected are available as the Data behind the Figure.

wide binary sample used in Mann et al. (2013) did not have stars outside this parameter space. The majority of stars in both our planet sample and field M dwarf sample are within these ranges (see Figure 4) so we consider the outliers are not expected to significantly impact the final results.

4.2. Refined Stellar and Planet Properties

In this section, we obtain the stellar properties of our planet sample in a homogeneous way to refine the planet

parameters, which enables the investigation of the relation between stellar metallicity and other planet properties. In short, we apply the empirical relations, calibrated with nearby binaries, between stellar physical parameters and absolute magnitude as well as color.

Combining the parallax from Gaia DR3 (Gaia Collaboration et al. 2023) and m_K magnitude from 2MASS (Cutri et al. 2003; Skrutskie et al. 2006), we first computed the absolute magnitude M_K of each M dwarf in our sample. The stellar masses M_* were then estimated

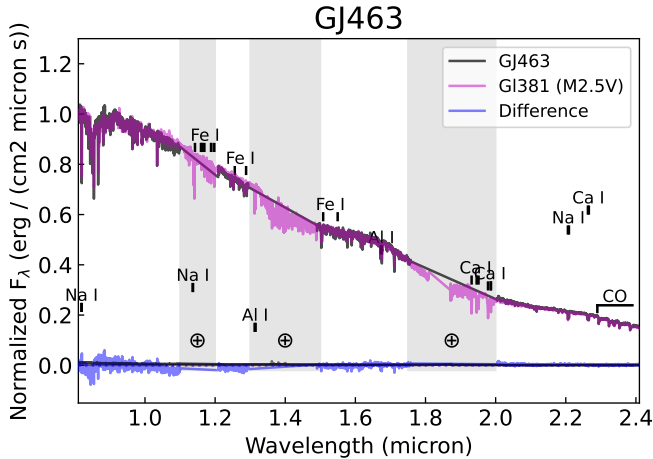


Figure 3. An example plot of spectrum match in Section 4. The black solid line is the normalized SpeX near-infrared spectrum of the target star GJ 463 while the best-match comparison spectrum taken from the IRTF library (Rayner et al. 2009) is shown in magenta. Strong atomic and molecular features are marked. The residuals (blue) are presented below.

through the M_* - M_K relation² derived by Mann et al. (2019), which is suitable for stars spanning a mass range of $0.075 \leq M_* \leq 0.7 M_\odot$ with a systematic uncertainty of about 3%. Since the effect of $[\text{Fe}/\text{H}]$ on the M_* - M_K relation is weak, about $0.0 \pm 2.2\%$ change in mass per dex change in $[\text{Fe}/\text{H}]$ for stars in the solar neighborhood (Mann et al. 2019), we do not take metallicity into account here. In terms of stellar radius R_* , we employed the third-order polynomial relation between R_* and M_K (see Eq. 4 in Mann et al. 2015). This relation is valid for stars that have spectral types ranging from K7 to M7 with a precision of 3%.

Furthermore, we estimated the stellar effective temperature using the T_{eff} -color relation reported in Mann et al. (2015). We retrieved the V -band magnitudes from APASS (Henden et al. 2016) and JH -magnitudes from 2MASS (Cutri et al. 2003; Skrutskie et al. 2006). We opted to use the relation that includes two stellar color terms $V - J$ and $J - H$, which gives a scatter of about 50 K. Combined with the typical spectroscopic error, we conservatively adopt a systematic uncertainty of 70 K. The final uncertainties of M_* , R_* , and T_{eff} are determined through error propagation after accounting for the aforementioned systematic errors of the methodology. We provide the information of the field M star catalog in Table 1 with each column described in Ta-

² <https://github.com/awmann/M-M-K->

ble 2. The stellar properties of our planet sample are listed in Table 3.

Finally, we recalculated the planetary mass M_p , semi-major axis a , and equilibrium temperature T_{eq} using the updated stellar properties above together with the orbital results from the literature. For each planet, we randomly draw a set of parameters including effective temperature T_{eff} , stellar mass M_* and radius R_* , period P , eccentricity e , and radial velocity semi-amplitude K from normal distributions, centered at the best-fits with σ adopted as the higher value of their lower and upper uncertainty to be conservative. We fixed the eccentricity at zero if the published result is 1) smaller than 0.1 and consistent with 0 within 3σ ; or 2) only an upper limit. We repeated the sampling process 5000 times, and recorded the median and standard deviation of each distribution as the final value and uncertainty of planetary parameters. Here, we do not induce the constraint on the scaled semi-major axis a/R_* from the light curve so the uncertainty is higher for transiting systems compared with the value in literature. Table 4 summarizes the refined planet properties of our planet sample.

5. DISCUSSIONS

5.1. Giant Planets Favor Metal-Rich M Dwarfs

With the $[\text{Fe}/\text{H}]$ and $[\text{M}/\text{H}]$ homogeneously measured based on spectral data from the same instrument through the same methodology, we investigate the metallicity distribution of the two samples we constructed. Since the behaviors of $[\text{Fe}/\text{H}]$ and $[\text{M}/\text{H}]$ are almost identical, we mainly focus on $[\text{Fe}/\text{H}]$ in the following sections and put all results of $[\text{M}/\text{H}]$ in the Appendix.

Figure 5 illustrates the iron abundance distribution and the corresponding cumulative function of field M dwarfs (black line) and M stars with confirmed giant planets (orange line) from two bands. Each two-giant-planet system is treated as two single-planet systems independently. We also repeat the same analysis below but treat those M dwarfs hosting two giant planets as single stars, which gives similar results. By visual inspection, it appears that giant planets were mostly found around metal-rich M dwarfs, suggesting a correlation between their formation and stellar metallicity, similar to FGK counterparts (Santos et al. 2004; Fischer & Valenti 2005; Johnson et al. 2010; Sousa et al. 2011; Maldonado et al. 2020; Osborn & Bayliss 2020). In addition, the iron abundance of M dwarfs harboring giant planets tends to show a bimodal distribution with one peak roughly located at the median $[\text{Fe}/\text{H}]$ of field M dwarfs and the other at about 0.4 dex. However, the two-peak phenomenon is not seen in $[\text{M}/\text{H}]$ (see Fig-

Table 1. Field M Dwarf Catalog. The descriptions of each column are presented in Table 2.

ID	μ_{α}	μ_{δ}	ϖ	V	J	H	K	SpT	MFeSH	MFeHK	MMHH	MMHK	M_*	R_*	T_{eff}
J00063925-0705354	-104.95 ± 0.43	119.32 ± 0.26	46.96 ± 0.40	14.71 ± 0.03	9.83 ± 0.03	9.26 ± 0.03	8.96 ± 0.02	5.46	-0.31	-0.02	-0.17	-0.08	0.25 ± 0.02	0.28 ± 0.02	3078 ± 83
J00102561+6212374	-28.68 ± 0.02	31.44 ± 0.02	37.88 ± 0.02	13.80 ± 0.02	9.65 ± 0.02	9.09 ± 0.02	8.81 ± 0.01	3.49	-0.11	0.17	-0.04	0.06	0.33 ± 0.02	0.35 ± 0.02	3288 ± 79
J00115302+2259047	119.50 ± 0.07	-212.39 ± 0.07	48.83 ± 0.06	13.00 ± 0.04	8.86 ± 0.02	8.31 ± 0.04	7.99 ± 0.02	3.62	0.09	0.25	0.04	0.14	0.37 ± 0.02	0.38 ± 0.02	3285 ± 83
J00161607+1951515	708.14 ± 0.04	-748.88 ± 0.04	65.05 ± 0.04	13.55 ± 0.20	8.89 ± 0.03	8.34 ± 0.04	8.10 ± 0.03	4.44	-0.03	-0.07	-0.15	-0.09	0.27 ± 0.02	0.29 ± 0.02	3130 ± 102
J00165029+0507261	-89.93 ± 0.04	-623.93 ± 0.03	56.16 ± 0.04	13.81 ± 0.02	9.40 ± 0.02	8.87 ± 0.05	8.59 ± 0.02	4.52	-0.17	-0.1	-0.19	-0.11	0.25 ± 0.02	0.27 ± 0.02	3190 ± 85
J00182256+4401222	2891.52 ± 0.01	411.83 ± 0.01	280.71 ± 0.02	8.09 ± 0.10	5.25 ± 0.26	4.48 ± 0.20	4.02 ± 0.02	1.89	-0.23	-0.28	-0.25	-0.18	0.40 ± 0.02	0.41 ± 0.03	3968 ± 307
J00182549+4401376	2862.80 ± 0.02	336.43 ± 0.02	280.69 ± 0.03	11.33 ± 0.20	6.79 ± 0.02	6.19 ± 0.02	5.95 ± 0.02	4.10	-0.13	-0.13	-0.14	-0.1	0.16 ± 0.02	0.20 ± 0.02	3200 ± 99
J00243478+3002295	585.89 ± 0.05	9.96 ± 0.03	51.32 ± 0.04	14.52 ± 0.07	9.78 ± 0.02	9.22 ± 0.02	8.89 ± 0.02	4.70	0.17	0.23	0.16	0.1	0.23 ± 0.02	0.26 ± 0.02	3115 ± 82
J00252063+2253121	-234.41 ± 0.04	-463.95 ± 0.03	61.90 ± 0.03	14.25 ± 0.06	9.72 ± 0.02	9.15 ± 0.02	8.87 ± 0.02	4.71	-0.11	-0.01	-0.18	-0.04	0.19 ± 0.02	0.23 ± 0.02	3182 ± 81
J00270673+4941531	367.63 ± 0.02	-224.69 ± 0.02	44.81 ± 0.03	14.19 ± 0.04	9.73 ± 0.02	9.16 ± 0.02	8.85 ± 0.02	4.00	0.14	0.25	0.07	0.15	0.27 ± 0.02	0.30 ± 0.02	3202 ± 80
J00283948-0639481	-327.79 ± 0.05	-800.63 ± 0.03	74.71 ± 0.04	12.50 ± 0.20	8.04 ± 0.02	7.50 ± 0.06	7.19 ± 0.02	4.18	-0.25	-0.24	-0.23	-0.13	0.35 ± 0.02	0.37 ± 0.02	3182 ± 106
J00294322+0112384	-171.70 ± 0.03	-147.50 ± 0.03	32.25 ± 0.03	12.28 ± 0.02	9.15 ± 0.02	8.54 ± 0.04	8.31 ± 0.02	1.75	-0.27	-0.16	-0.24	-0.15	0.46 ± 0.03	0.47 ± 0.03	3700 ± 84
J00312156+0009294	522.22 ± 0.03	111.05 ± 0.02	32.90 ± 0.03	13.62 ± 0.02	9.76 ± 0.02	9.16 ± 0.03	8.90 ± 0.02	3.23	-0.09	0.12	-0.05	0.03	0.36 ± 0.02	0.38 ± 0.02	3408 ± 81
J00313539-0552115	350.97 ± 0.04	-1055.47 ± 0.03	71.02 ± 0.03	12.87 ± 0.20	8.76 ± 0.03	8.22 ± 0.03	7.95 ± 0.02	3.68	-0.24	-0.11	-0.22	-0.1	0.26 ± 0.02	0.29 ± 0.02	3288 ± 103
J00321574+5429027	-208.27 ± 0.02	-441.04 ± 0.02	49.95 ± 0.03	13.86 ± 0.03	9.39 ± 0.02	8.83 ± 0.02	8.57 ± 0.01	4.49	0.0	-0.04	-0.08	-0.05	0.28 ± 0.02	0.30 ± 0.02	3193 ± 80
J00325313-0434068	81.75 ± 0.12	-131.34 ± 0.09	52.85 ± 0.10	14.00 ± 0.03	9.28 ± 0.02	8.62 ± 0.03	8.35 ± 0.02	4.83	-0.04	0.24	0.1	0.11	0.29 ± 0.02	0.31 ± 0.02	3189 ± 81
J00383388+5127579	-228.57 ± 0.03	35.54 ± 0.03	55.83 ± 0.03	12.62 ± 0.05	8.89 ± 0.03	8.34 ± 0.02	8.06 ± 0.02	2.83	-0.28	-0.17	-0.23	-0.15	0.32 ± 0.02	0.34 ± 0.02	3418 ± 83
J00391896+5508132	-360.78 ± 0.02	-234.31 ± 0.02	58.19 ± 0.02	14.19 ± 0.03	10.02 ± 0.02	9.52 ± 0.02	9.24 ± 0.02	4.05	-0.32	-0.4	-0.38	-0.32	0.17 ± 0.02	0.21 ± 0.02	3244 ± 79
J00393349+1454188	331.91 ± 0.03	34.95 ± 0.03	34.82 ± 0.03	14.57 ± 0.20	9.96 ± 0.03	9.40 ± 0.03	9.12 ± 0.02	4.01	0.15	0.15	0.08	0.09	0.31 ± 0.02	0.33 ± 0.02	3151 ± 101
J00393374+1454348	327.54 ± 0.25	29.75 ± 0.21	34.26 ± 0.22	14.71 ± 0.20	9.83 ± 0.03	9.22 ± 0.03	8.95 ± 0.02	4.67	0.0	0.28	0.08	0.15	0.34 ± 0.02	0.36 ± 0.02	3107 ± 101
J00393379+6033153	-157.75 ± 0.03	-292.62 ± 0.04	27.12 ± 0.03	12.80 ± 0.05	9.20 ± 0.02	8.58 ± 0.02	8.34 ± 0.02	2.42	0.08	0.31	0.1	0.19	0.52 ± 0.03	0.52 ± 0.03	3510 ± 81
J00405623+3122565	-42.77 ± 0.04	-331.45 ± 0.03	44.39 ± 0.03	13.86 ± 0.07	9.49 ± 0.02	8.86 ± 0.03	8.59 ± 0.02	3.33	0.15	0.56	0.07	0.38	0.31 ± 0.02	0.33 ± 0.02	3273 ± 83
J00412078+5550044	324.33 ± 0.01	-73.26 ± 0.02	43.73 ± 0.02	14.77 ± 0.20	9.84 ± 0.02	9.31 ± 0.02	9.04 ± 0.02	4.17	-0.15	-0.19	-0.19	-0.16	0.26 ± 0.02	0.28 ± 0.02	3038 ± 98
J00442070+0907345	813.09 ± 0.10	-2.55 ± 0.07	40.01 ± 0.08	14.47 ± 0.20	9.50 ± 0.03	8.96 ± 0.03	8.62 ± 0.02	4.48	0.07	0.19	-0.01	0.08	0.34 ± 0.02	0.36 ± 0.02	3033 ± 100
J00462990+5038389	419.18 ± 0.02	-213.83 ± 0.02	30.95 ± 0.02	14.34 ± 0.02	9.96 ± 0.02	9.33 ± 0.02	9.07 ± 0.02	3.25	0.27	0.44	0.19	0.32	0.36 ± 0.02	0.37 ± 0.02	3268 ± 79
J00501752+0837341	66.96 ± 0.07	-35.13 ± 0.04	16.31 ± 0.05	14.35 ± 0.04	9.74 ± 0.02	9.15 ± 0.02	8.90 ± 0.02	5.14	-0.04	-0.05	-0.14	-0.09	0.60 ± 0.03	0.62 ± 0.03	3171 ± 80
J00523518+4712433	260.33 ± 0.02	76.84 ± 0.02	31.25 ± 0.03	13.98 ± 0.20	9.76 ± 0.02	9.19 ± 0.02	8.93 ± 0.02	3.30	-0.09	-0.04	-0.09	-0.06	0.38 ± 0.02	0.39 ± 0.02	3275 ± 100
J00563841+1727347	683.34 ± 0.05	-291.75 ± 0.04	54.85 ± 0.04	13.73 ± 0.03	9.28 ± 0.02	8.65 ± 0.03	8.37 ± 0.03	3.78	0.17	0.57	0.09	0.37	0.28 ± 0.02	0.30 ± 0.02	3247 ± 81
J00580115+3919111	-107.05 ± 0.03	25.00 ± 0.02	68.39 ± 0.04	14.17 ± 0.03	9.56 ± 0.03	8.95 ± 0.03	8.68 ± 0.02	4.23	-0.16	-0.03	-0.07	-0.05	0.19 ± 0.02	0.22 ± 0.02	3186 ± 83
J01004948+6656546	-236.24 ± 0.02	-54.67 ± 0.02	44.32 ± 0.02	13.43 ± 0.02	9.41 ± 0.03	8.73 ± 0.03	8.48 ± 0.02	3.50	0.12	0.24	0.1	0.18	0.33 ± 0.02	0.35 ± 0.02	3415 ± 83

(The full table including 746 stars is available in its entirety in the machine-readable format. A portion is shown here for guidance regarding its form and content.)

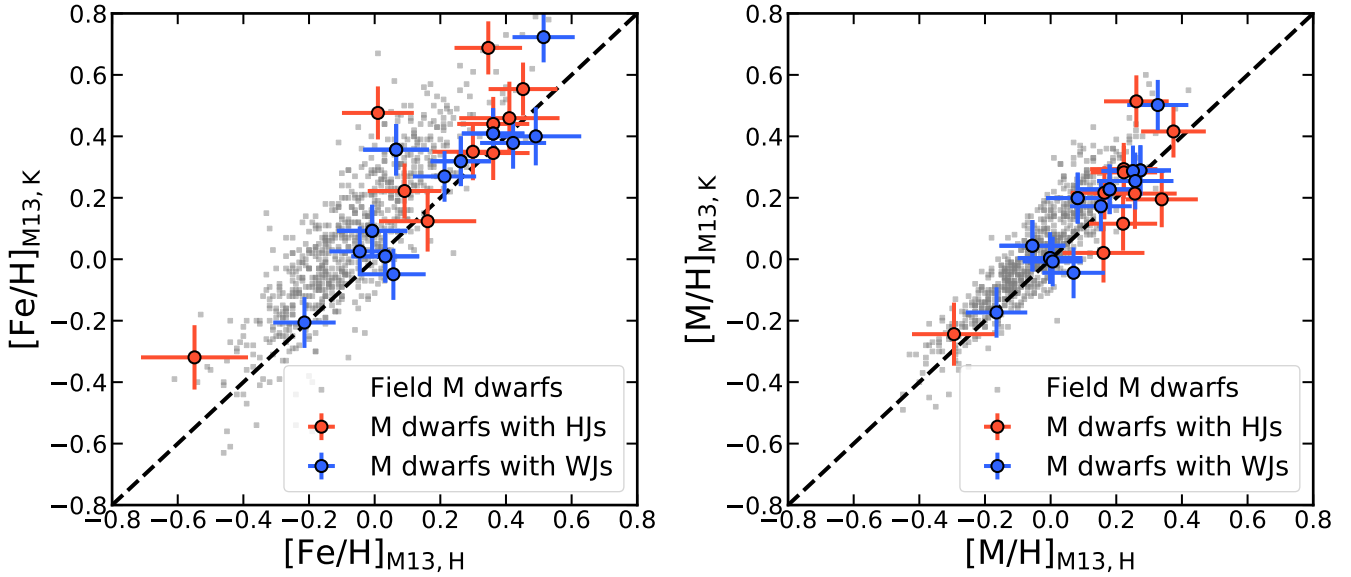


Figure 4. Comparisons of $[\text{Fe}/\text{H}]$ (left) and $[\text{M}/\text{H}]$ (right) between H -band and K -band measurements. The background grey dots are the field M stars. The red and blue dots are the M dwarfs with hot and warm Jupiters with scaled semi-major axis $a/R_* \leq 20$ and $a/R_* > 20$, respectively. The systematic errors of 0.09 and 0.08 dex of the H and K band calibration have been taken into account. The black dashed line marks the one-to-one function.

Table 2. Field M Dwarf Catalog Column Descriptions.

Name	Description	Ref.
ID	2MASS Identifier	2MASS ^[1]
μ_α (mas yr ⁻¹)	Gaia Proper Motion in R.A.	Gaia DR3 ^[2]
μ_δ (mas yr ⁻¹)	Gaia Proper Motion in Decl.	Gaia DR3
ϖ (mas)	Gaia Parallax	Gaia DR3
V (mag)	APASS V Band Magnitude	APASS ^[3]
J (mag)	2MASS J Band Magnitude	2MASS
H (mag)	2MASS H Band Magnitude	2MASS
K (mag)	2MASS K Band Magnitude	2MASS
SpT	M Spectral Subtype defined in Newton et al. (2014)	Terrien et al. (2015)
MFeHH (dex)	$[\text{Fe}/\text{H}]$ from H -band defined in Mann et al. (2013), denoted as $[\text{Fe}/\text{H}]_{\text{M13,H}}$	Terrien et al. (2015)
MFeHK (dex)	$[\text{Fe}/\text{H}]$ from K -band defined in Mann et al. (2013), denoted as $[\text{Fe}/\text{H}]_{\text{M13,K}}$	Terrien et al. (2015)
MMHH (dex)	$[\text{M}/\text{H}]$ from H -band defined in Mann et al. (2013), denoted as $[\text{M}/\text{H}]_{\text{M13,H}}$	Terrien et al. (2015)
MMHK (dex)	$[\text{M}/\text{H}]$ from K -band defined in Mann et al. (2013), denoted as $[\text{M}/\text{H}]_{\text{M13,K}}$	Terrien et al. (2015)
M_* (M_\odot)	Stellar Mass from M_* - M_K Relation in Mann et al. (2019)	This Work
R_* (R_\odot)	Stellar Radius from R_* - M_K Relation in Mann et al. (2015)	This Work
T_{eff} (K)	Stellar Effective Temperature from T_{eff} -Color Relation in Mann et al. (2015) ^[4]	This Work

[1] Cutri et al. (2003); Skrutskie et al. (2006); [2] Gaia Collaboration et al. (2023); [3] Henden et al. (2016); [4] We use the empirical relation that includes two color terms: $V - J$ and $J - H$.

Table 3. Stellar Properties of the M Dwarf Giant Planet Sample.

Target (2MASS ID)	Other Identifier	SpT	[Fe/H] _{M13,H}	[Fe/H] _{M13,K}	[M/H] _{M13,H}	[M/H] _{M13,K}	M_* (M_\odot)	R_* (R_\odot)	T_{eff} (K)
J11414471+4245072	GJ 1148 ^[1]	4.5	0.03 ± 0.10	0.01 ± 0.08	-0.00 ± 0.10	0.00 ± 0.08	0.34 ± 0.02	0.36 ± 0.02	3220 ± 80
J04520573+0628356	GJ 179 ^[2]	4.5	0.21 ± 0.09	0.27 ± 0.08	0.15 ± 0.09	0.17 ± 0.08	0.36 ± 0.02	0.38 ± 0.02	3321 ± 86
J08405923-2327232	GJ 317 ^[3]	4.5	0.07 ± 0.10	0.36 ± 0.08	0.08 ± 0.09	0.20 ± 0.08	0.42 ± 0.03	0.43 ± 0.03	3231 ± 110
J08412013+5929505	GJ 3512 ^[4]	5.0	-0.01 ± 0.11	0.09 ± 0.08	-0.06 ± 0.10	0.04 ± 0.08	0.13 ± 0.02	0.16 ± 0.02	2927 ± 94
J12230024+6401506	GJ 463 ^[5]	2.5	0.06 ± 0.10	-0.05 ± 0.08	0.07 ± 0.09	-0.04 ± 0.08	0.47 ± 0.03	0.47 ± 0.03	3473 ± 83
J16580884+2544392	GJ 649 ^[6]	2.0	-0.05 ± 0.09	0.03 ± 0.08	0.01 ± 0.09	-0.01 ± 0.08	0.51 ± 0.03	0.52 ± 0.03	3624 ± 91
J22094029-0438267	GJ 849 ^[7]	4.5	0.36 ± 0.09	0.41 ± 0.08	0.27 ± 0.09	0.29 ± 0.08	0.46 ± 0.03	0.46 ± 0.03	3403 ± 90
J22531672-1415489	GJ 876 ^[8]	4.5	0.26 ± 0.09	0.32 ± 0.08	0.18 ± 0.09	0.23 ± 0.08	0.34 ± 0.02	0.35 ± 0.02	3283 ± 90
J05523523-1901539	HATS-6 ^[9]	1.0	0.36 ± 0.10	0.35 ± 0.09	0.16 ± 0.10	0.22 ± 0.08	0.59 ± 0.03	0.60 ± 0.03	3791 ± 94
J04034783-2524320	HATS-75 ^[10]	0.5	0.30 ± 0.12	0.35 ± 0.09	0.34 ± 0.10	0.19 ± 0.09	0.58 ± 0.03	0.59 ± 0.03	3745 ± 110
J16124178-1852317	HIP 79431 ^[11]	1.5	0.51 ± 0.09	0.72 ± 0.08	0.33 ± 0.09	0.50 ± 0.08	0.48 ± 0.03	0.48 ± 0.03	3487 ± 87
J19312949+4103513	Kepler-45 ^[12]	1.5	0.41 ± 0.15	0.46 ± 0.12	0.26 ± 0.13	0.21 ± 0.11	0.60 ± 0.03	0.62 ± 0.03	3810 ± 110
J05305145-3637508	NGTS-1 ^[13]	1.0	-0.55 ± 0.17	-0.32 ± 0.11	-0.29 ± 0.13	-0.24 ± 0.10	0.56 ± 0.03	0.57 ± 0.03	3805 ± 110
J19574239+4008357	TOI-1899 ^[14]	0.5	0.42 ± 0.10	0.38 ± 0.08	0.25 ± 0.09	0.29 ± 0.08	0.60 ± 0.03	0.62 ± 0.03	3574 ± 110
J23591015+3918514	TOI-3629 ^[15]	0.0	0.45 ± 0.10	0.55 ± 0.08	0.37 ± 0.10	0.42 ± 0.08	0.60 ± 0.03	0.62 ± 0.03	3717 ± 87
J04381253+3927299	TOI-3714 ^[16]	1.5	0.01 ± 0.11	0.48 ± 0.08	0.22 ± 0.10	0.29 ± 0.08	0.51 ± 0.03	0.51 ± 0.03	3431 ± 101
J06040089+5501126	TOI-3757 ^[17]	0.0	0.09 ± 0.11	0.22 ± 0.09	0.22 ± 0.10	0.12 ± 0.09	0.62 ± 0.03	0.64 ± 0.03	3925 ± 92
J06015391-1327410	TOI-4201 ^[18]	1.5	0.36 ± 0.11	0.44 ± 0.09	0.22 ± 0.10	0.28 ± 0.08	0.60 ± 0.03	0.62 ± 0.03	3874 ± 92
J08182567-1939465	TOI-519 ^[19]	4.5	0.16 ± 0.15	0.12 ± 0.10	0.16 ± 0.13	0.02 ± 0.09	0.34 ± 0.02	0.36 ± 0.02	3225 ± 100
J20550491+2421387	TOI-5205 ^[20]	4.5	0.35 ± 0.10	0.69 ± 0.08	0.26 ± 0.10	0.51 ± 0.08	0.39 ± 0.02	0.40 ± 0.02	3433 ± 110
J06533906+1252545	TOI-530 ^[21]	1.5	0.49 ± 0.14	0.40 ± 0.09	0.26 ± 0.11	0.25 ± 0.09	0.54 ± 0.03	0.55 ± 0.03	3650 ± 100
J21220626+2255531	TYC 2187-512-1 ^[22]	2.0	-0.21 ± 0.09	-0.21 ± 0.08	-0.16 ± 0.09	-0.17 ± 0.08	0.50 ± 0.03	0.50 ± 0.03	3668 ± 86

[1] Haghhighipour et al. (2010); Trifonov et al. (2018); Rosenthal et al. (2021); [2] Howard et al. (2010); Rosenthal et al. (2021); [3] Johnson et al. (2007); Anglada-Escudé et al. (2012); Rosenthal et al. (2021); [4] Morales et al. (2019); Lopez-Santiago et al. (2020); [5] Endl et al. (2022); Sozzetti (2023); [6] Johnson et al. (2010); Rosenthal et al. (2021); Pinamonti et al. (2023); [7] Butler et al. (2006); Bonfils et al. (2013); Rosenthal et al. (2021); Pinamonti et al. (2023); [8] Marcy et al. (1998); Correia et al. (2010); Rivera et al. (2010); Trifonov et al. (2018); Rosenthal et al. (2021); [9] Hartman et al. (2015); [10] Jordán et al. (2022); [11] Apps et al. (2010); [12] Johnson et al. (2012); Bonomo et al. (2017); [13] Bayliss et al. (2018); [14] Cañas et al. (2020); Lin et al. (2023); [15] Cañas et al. (2022); Hartman et al. (2023); [16] Cañas et al. (2022); Hartman et al. (2023); [17] Kanodia et al. (2022); [18] Gan et al. (2023b); Hartman et al. (2023); Delamer et al. (2024); [19] Parviainen et al. (2021); Kageitani et al. (2023); Hartman et al. (2023); [20] Kanodia et al. (2023); [21] Gan et al. (2022); [22] Quirrenbach et al. (2022)

ure 9). Since the planet number in each [Fe/H] bin is small, we attribute the feature to Poisson noise and do not over-interpret it.

To statistically examine whether the field M dwarfs and M stars hosting giant planets have an identical underlying [Fe/H] distribution, we carry out Kolmogorov-Smirnov (K-S; Hodges 1958) and Anderson-Darling (A-D; Scholz & Stephens 1987) tests. As the sample sizes are small, we apply the permutation method for the A-D test to obtain accurate p -values with the number of resamples set to 10^6 . We calculate the K-S and A-D statistic between two samples using the functions embedded in SciPy (Virtanen et al. 2020), which yield p -values of 4.9×10^{-7} and 9.9×10^{-7} for the H -band as well as 6.3×10^{-5} and 4.2×10^{-5} for the K -band metallicities, corresponding to 5σ and 4σ significance, respectively. To account for the uncertainty of each metallicity measurement, we resample the [Fe/H]_{M13,H} and [Fe/H]_{M13,K} by randomly drawing samples, assuming Gaussian distributions $\mathcal{N}([\text{Fe}/\text{H}], \sigma_{[\text{Fe}/\text{H}]})$. Since the metallicity uncertainty of the field star data set is unavailable in Terrien et al. (2015), we assign 0.09 dex and 0.08 dex sys-

tematical errors³ to the H and K band measurements before randomizing. We loop the procedure 10000 times, record the p -values, and compute the fraction of trials with $p \leq 0.003$, corresponding to the 3σ significance criterion. We list all details of the K-S along with the A-D tests in Table 5. To sum up, we find that nearly all trials lead to p -values smaller than the 0.003 threshold, hence indicating a strong significance. Therefore, we conclude that the null hypothesis, the iron abundance distributions of field M dwarfs and M stars with giant planets are the same, could be rejected. Our findings suggest that giant planets favor metal-rich M stars, which agree with the conclusions from previous studies (Johnson & Apps 2009; Rojas-Ayala et al. 2010).

5.2. Metallicity Preference of Hot and Warm Jupiters

Some initial efforts found that hot and warm Jupiters around M dwarfs may have different preferences of stellar metallicity (Gan et al. 2022, 2023b), hinting at different formation histories (Pollack et al. 1996; Boss 2002).

³ These systematical errors of the methodology dominate the final uncertainty according to our findings based on the planet sample (see Table 3).

Table 4. Planet Properties of the M Dwarf Giant Planet Sample.

Planet	$M_p \sin i$ (M_{Jup})	Mass Ratio	a (AU)	$a/R_*^{[1]}$	T_{eq} (K) ^[2]	Group ^[3]
GJ 1148b	0.297 ± 0.007	0.000823 ± 0.000145	0.1641 ± 0.0017	98.20 ± 16.82	229 ± 20	WJ
GJ 1148c	0.208 ± 0.013	0.000577 ± 0.000107	0.9010 ± 0.0098	539.20 ± 92.40	98 ± 15	WJ
GJ 179b	0.828 ± 0.074	0.002171 ± 0.000416	2.4266 ± 0.0476	1386.49 ± 233.28	63 ± 12	WJ
GJ 317b	1.753 ± 0.037	0.003973 ± 0.000676	1.1530 ± 0.0111	580.11 ± 97.41	94 ± 15	WJ
GJ 317c	1.644 ± 0.044	0.003726 ± 0.000637	5.2375 ± 0.0888	2635.17 ± 444.01	44 ± 10	WJ
GJ 3512b	0.474 ± 0.011	0.003534 ± 0.000668	0.3419 ± 0.0040	470.82 ± 146.10	95 ± 15	WJ
GJ 3512c	0.220 ± 0.006	0.001643 ± 0.000311	1.3491 ± 0.0159	1857.95 ± 576.54	47 ± 10	WJ
GJ 463b	1.500 ± 0.139	0.003027 ± 0.000583	3.4826 ± 0.0732	1575.16 ± 236.52	61 ± 12	WJ
GJ 649b	0.259 ± 0.014	0.000480 ± 0.000086	1.1155 ± 0.0110	463.54 ± 61.33	118 ± 15	WJ
GJ 849b	0.908 ± 0.029	0.001880 ± 0.000327	2.3415 ± 0.0232	1084.16 ± 163.44	73 ± 13	WJ
GJ 849c	1.002 ± 0.047	0.002075 ± 0.000368	4.9890 ± 0.0745	2309.97 ± 349.20	50 ± 10	WJ
GJ 876b	1.988 ± 0.042	0.005629 ± 0.001001	0.2115 ± 0.0022	129.07 ± 25.31	204 ± 10	WJ
GJ 876c	0.656 ± 0.014	0.001858 ± 0.000330	0.1322 ± 0.0014	80.69 ± 15.82	258 ± 10	WJ
HATS-6b	0.325 ± 0.073	0.000528 ± 0.000150	0.0365 ± 0.0004	13.09 ± 2.08	740 ± 20	HJ
HATS-75b	0.478 ± 0.039	0.000788 ± 0.000153	0.0323 ± 0.0003	11.79 ± 1.89	771 ± 25	HJ
HIP 79431b	2.068 ± 0.058	0.004138 ± 0.000743	0.3550 ± 0.0040	159.24 ± 23.64	195 ± 15	WJ
Kepler-45b	0.516 ± 0.048	0.000817 ± 0.000161	0.0301 ± 0.0003	10.48 ± 2.18	834 ± 30	HJ
NGTS-1b	0.770 ± 0.053	0.001305 ± 0.000241	0.0309 ± 0.0003	11.66 ± 1.98	787 ± 25	HJ
TOI-1899b	0.646 ± 0.040	0.001023 ± 0.000188	0.1564 ± 0.0016	54.29 ± 7.09	343 ± 10	WJ
TOI-3629b	0.249 ± 0.023	0.000395 ± 0.000077	0.0412 ± 0.0004	14.36 ± 2.13	693 ± 18	HJ
TOI-3714b	0.682 ± 0.025	0.001283 ± 0.000226	0.0260 ± 0.0003	10.97 ± 1.68	732 ± 23	HJ
TOI-3757b	0.263 ± 0.028	0.000405 ± 0.000081	0.0380 ± 0.0004	12.77 ± 1.96	776 ± 21	HJ
TOI-4201b	2.446 ± 0.084	0.003883 ± 0.000685	0.0387 ± 0.0004	13.50 ± 2.21	745 ± 20	HJ
TOI-519b	0.471 ± 0.087	0.001318 ± 0.000335	0.0160 ± 0.0002	9.65 ± 2.17	733 ± 29	HJ
TOI-5205b	1.068 ± 0.048	0.002614 ± 0.000474	0.0198 ± 0.0002	10.70 ± 2.08	740 ± 28	HJ
TOI-530b	0.405 ± 0.086	0.000713 ± 0.000195	0.0550 ± 0.0006	21.62 ± 3.59	554 ± 17	WJ
TYC 2187-512-1b	0.328 ± 0.014	0.000629 ± 0.000113	1.2137 ± 0.0155	521.48 ± 85.95	113 ± 10	WJ

[1] The uncertainties on the scaled semi-major axis a/R_* of transiting systems are higher than literature values because here we do not use constraint from the light curve. [2] We do not consider heat distribution between the dayside and nightside here and assume albedo $A_B = 0$. [3] The hot Jupiter (HJ) and warm Jupiter (WJ) groups are designated as giant planets ($M_p > 0.2 M_{\text{Jup}}$) with $a/R_* \leq 20$ and $a/R_* > 20$.

However, the large uncertainty of $[\text{Fe}/\text{H}]$ as well as the systematic biases from heterogeneous instruments and methodologies that are challenging to characterize impede these works to draw a robust conclusion. Here, we revisit the puzzle using our samples characterized through a uniform pathway.

We divide the full giant planet sample into two subclasses: hot and warm Jupiters based on the refined planet properties. Following [Gan et al. \(2023b\)](#), we designate hot Jupiters (HJ) as planets having $M_p \geq 0.2 M_{\text{Jup}}$ and $a/R_* \leq 20$ and warm Jupiters (WJ) as planets within the same mass range but $a/R_* > 20$. In this way, we find 10 HJs and 17 WJs, including 5 multi-warm Jupiter systems. Among two groups, there are one HJ and one WJ whose host stars plausibly have sub-solar metallicities: NGTS-1 ($[\text{Fe}/\text{H}]_{\text{M13,H}} = -0.55 \pm 0.17$ dex, $[\text{Fe}/\text{H}]_{\text{M13,K}} = -0.32 \pm 0.11$ dex)⁴ and TYC 2187-512-1 ($[\text{Fe}/\text{H}]_{\text{M13,H}} = -0.21 \pm 0.09$ dex,

$[\text{Fe}/\text{H}]_{\text{M13,K}} = -0.21 \pm 0.08$ dex)⁵. We present the metallicity distributions of two groups in Figure 5 (HJ: red line, WJ: blue line). We examine whether the HJ and WJ populations are similar to each other through the same method as in Section 5.1. We find that the p -values of both the K-S and A-D tests are approximately 10^{-1} . In fact, almost none of randomly drawn samples have p -values falling below 0.003. All results can be found in Table 5. Similar features are also seen for $[\text{M}/\text{H}]$ (see Table 6). Consequently, we are not able to reject the null hypothesis that two distributions are identical. At this point, we conclude that HJs and WJs present analogous preferences on the metallicity of their host M dwarfs. As an independent inspection, we vary the a/R_* boundary between 15 and 50 to define HJs and WJs and rerun the analysis. We find that the conclusion does not depend on the exact choice of a/R_* .

Next, we attempt to explore the iron abundance distribution of cold Jupiters (CJs). The reason is that

⁴ For NGTS-1, [Bayliss et al. \(2018\)](#) fixed an overall metallicity of $[\text{M}/\text{H}] = 0$ dex in the analysis but did not have an estimate on $[\text{Fe}/\text{H}]$.

⁵ For TYC 2187-512-1, [Quirrenbach et al. \(2022\)](#) reported two $[\text{Fe}/\text{H}]$ values: 0.08 ± 0.19 dex from [Passegger et al. \(2019\)](#) and -0.18 ± 0.08 dex from [Marfil et al. \(2021\)](#).

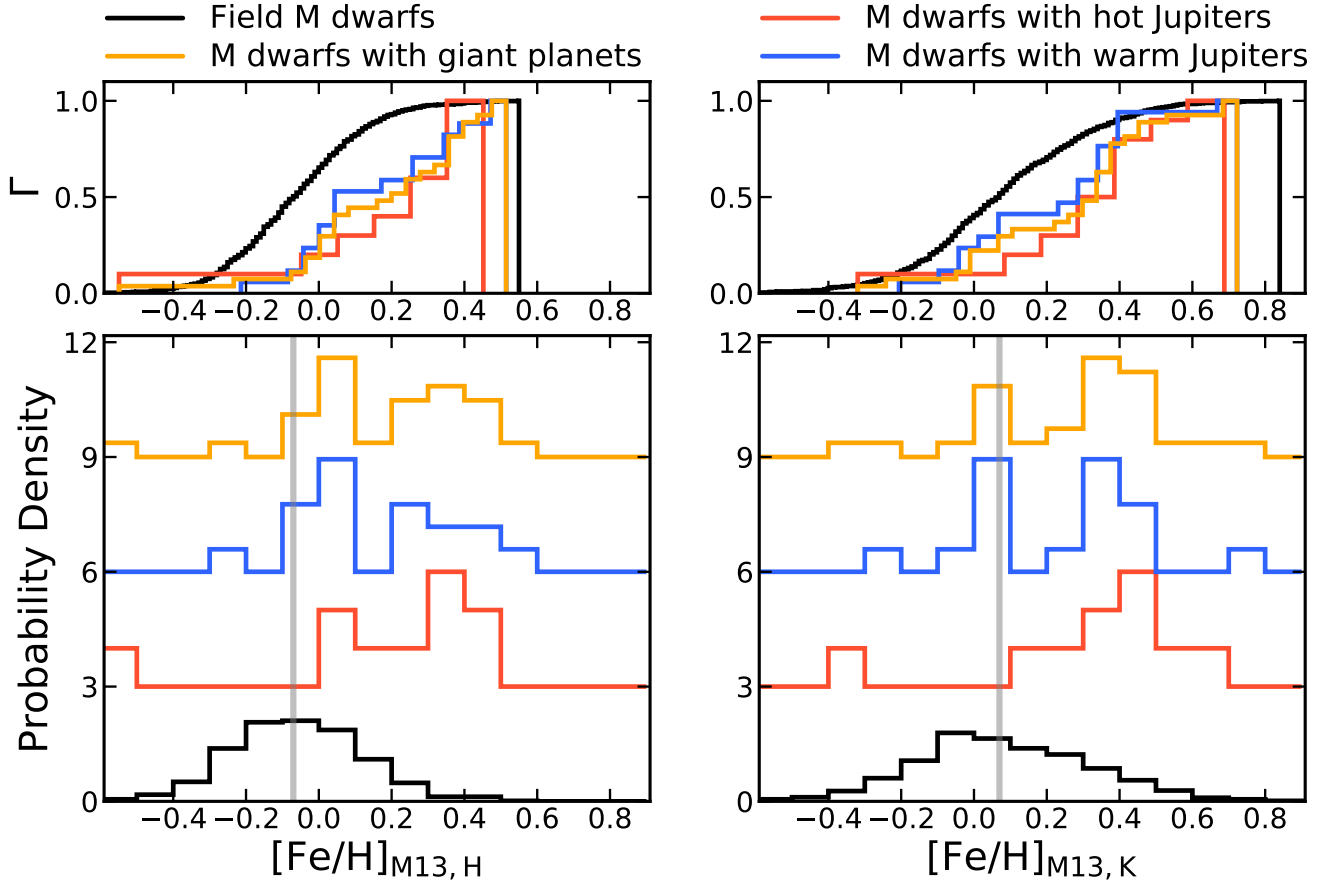


Figure 5. Metallicity distribution of the field M stars (black) and M dwarfs with giant planets (orange), either hot Jupiters (red) with $a/R_* \leq 20$ or warm Jupiters (blue) with $a/R_* > 20$. The left and right panels are the results from H - and K -band measurements. The vertical grey line in each panel marks the median $[\text{Fe}/\text{H}]$ of the field M dwarf sample, -0.07 and 0.07 dex. The cumulative functions are shown above. Most confirmed giant planets were orbiting metal-rich M stars. The tentative bimodal distribution of $[\text{Fe}/\text{H}]$ is likely due to Poisson noise.

planets formed through gravitational instability are generally located at several AUs away from the host star (Boss 2006). The massive gas giants could form around M dwarfs with relatively low metallicity in the context of such a framework (Boss 2002). If the inner HJs and outer CJs are from two formation channels, we might expect to spot a discrepancy in their metallicity distribution. We further separate wide-orbit Jupiters with scaled semi-major axis a/R_* larger than 200 from the original WJ sample, where we find 11 out of 17 planets belonging to this subgroup. The boundary of $a/R_* = 200$ here is chosen somewhat arbitrarily by visually inspecting the a/R_* distribution of our planet sample (see Figure 10 in the Appendix), where there is a blank of planets with a/R_* between 200 and 400. Figure 6 presents the cumulative $[\text{Fe}/\text{H}]$ and $[\text{M}/\text{H}]$ distributions of three categories: HJ ($a/R_* \leq 20$), WJ ($20 < a/R_* \leq 200$) and CJ ($a/R_* > 200$). Under this new classification above, we find that the CJs tentatively show a weaker dependence on metallicity compared with

HJs. The K-S and A-D tests show that the p -values vary between 4.4×10^{-3} and 2.6×10^{-1} , shown in Figure 6. If such a phenomenon turns out to be true, wide-orbit ($a \gtrsim 0.5$ AU) gas giants around M dwarfs perhaps have an origin different from close-in ($a \lesssim 0.05$ AU) analogues. Given the limited sample size, however, we do not intend to claim any trend at present. More detections of CJs through long-term near-infrared spectroscopic surveys are required to distinguish the metallicity difference between the HJ and the CJ population.

5.3. No Significant Correlation Between Stellar Metallicity and Planet Mass

Metal-rich stars are supposed to supply more solid materials supporting core accretion, and thus have the ability to form massive planets even around low-mass stars (Ida & Lin 2004b). In Figure 7, we plot the iron abundances versus refined planet masses and the planet-to-star mass ratios. We compute the Pearson correlation coefficients between the mass M_p of all giant planets in

Table 5. The p -values of K-S and A-D tests of the $[\text{Fe}/\text{H}]_{\text{M13,H}}$ (upper) as well as $[\text{Fe}/\text{H}]_{\text{M13,K}}$ (lower) distributions. Four groups are investigated including field M stars, M dwarfs with giant planets along with its two subgroups: hot ($a/R_* \leq 20$) and warm ($a/R_* > 20$) Jupiters. The value in the bracket is the fraction of randomly generated samples that have p -values smaller than 0.003 in our simulation (see Section 5). All bottom left results are from the K-S test while the results on the top right are from the A-D test.

$[\text{Fe}/\text{H}]_{\text{M13,H}}$	Field M	M + HJ	M + WJ	M + HJ or WJ
Field M	...	3.9×10^{-6} (99.2%)	1.9×10^{-6} (99.7%)	9.9×10^{-7} (100%)
M + HJ	3.9×10^{-4} (83.2%)	...	4.4×10^{-1} (0%)	...
M + WJ	1.4×10^{-4} (73.9%)	4.0×10^{-1} (0%)
M + HJ or WJ	4.9×10^{-7} (100%)
$[\text{Fe}/\text{H}]_{\text{M13,K}}$	Field M	M + HJ	M + WJ	M + HJ or WJ
Field M	...	4.1×10^{-4} (83.4%)	1.0×10^{-2} (49.2%)	4.2×10^{-5} (99.7%)
M + HJ	1.7×10^{-3} (60.1%)	...	1.4×10^{-1} (0%)	...
M + WJ	1.6×10^{-2} (24.4%)	1.2×10^{-1} (0.1%)
M + HJ or WJ	6.3×10^{-5} (95.2%)

the planet sample and the $[\text{Fe}/\text{H}]$ as well as $[\text{M}/\text{H}]$ of their host stars, and we find the p -values have a large scatter, varying between 0.01 and 0.9. As all p -values are greater than 0.003, we consider there is no significant correlation between stellar metallicity and planet mass. Nevertheless, we note that there seems to be a lack of giant planets with mass above $1 M_{\text{Jup}}$ around low-metallicity M stars, similar to giant planets around Sun-like stars (e.g., Fischer & Valenti 2005; Thorngren et al. 2016).

Additionally, massive hot Jupiters are rare around M dwarfs, manifesting as a lack of planets with $M_p \geq 1 M_{\text{Jup}}$ or $M_p/M_* \geq 2 \times 10^{-3}$. Moving outwards, radial velocity surveys have found several high-mass-ratio M dwarf-giant planet systems, probably due to observational bias. Multi-giant planets seem to always form far from the host M dwarfs, which have a similar $[\text{Fe}/\text{H}]$ distribution as M stars hosting a HJ or a single WJ.

5.4. Dependence on Stellar Mass

Theoretical simulations show that mid-to-late M dwarfs are even more challenging to form giant planets compared with early-M stars (e.g., Liu et al. 2019; Burn et al. 2021), which might be compensated by a higher metallicity. We thus investigate whether stellar mass impacts the planet-metallicity relation.

Figure 8 presents the iron abundance $[\text{Fe}/\text{H}]_{\text{M13,K}}$ and refined stellar mass of our M dwarf sample with confirmed giant planets as well as the field M star group. We find that the field M dwarfs mostly have a solar-like metallicity as their mass increases from 0.1 to $0.65 M_{\odot}$. Early-M dwarfs ($M_* > 0.4 M_{\odot}$) with giant planets have a wide range of metallicity, spanning from -0.4 to 0.7 dex. Both HJs and WJs have ever been detected around metal-poor early-M stars. Although mid-to-late M dwarfs ($M_* \leq 0.4 M_{\odot}$) hosting giant plan-

ets have solar-like or super-solar metallicities, these values are not significantly higher than those of field stars within the same stellar mass range and those early-M dwarfs with gas giants, but only a few such systems have been confirmed. Future discoveries of such systems shall remedy the situation and enable a detailed comparison between giant planets around early and mid-to-late M dwarfs.

6. CONCLUSIONS

In this work, we present the homogeneously derived stellar and planet properties of 22 M dwarfs hosting 27 giant planets with spectra collected by IRTF/SpEx. By comparing the metallicity distribution of this planet sample with a field M dwarf group analyzed following the same procedure, we find that giant planets have a strong preference to metal-rich M dwarfs ($4\text{-}5\sigma$ significance), similar to FGK counterparts. Meanwhile, we find no evidence of metallicity dependence difference between hot Jupiters ($a/R_* \leq 20$) and warm Jupiters ($a/R_* > 20$) around M dwarfs. A subsample with $a/R_* > 200$ that belongs to the warm-Jupiter group tends to have a weaker preference on both $[\text{Fe}/\text{H}]$ and $[\text{M}/\text{H}]$ compared with the hot Jupiter population. Based on the refined stellar and planetary physical parameters, we examine the stellar metallicities and planet masses and we find no significant correlation between them, which is yet to be confirmed given the limited sample size. Finally, M dwarfs with multi-giant planets and mid-to-late M dwarfs with giant planets do not show especially high metallicities compared with those hosting a single gas giant and those early-M dwarfs with giant planets.

7. ACKNOWLEDGMENTS

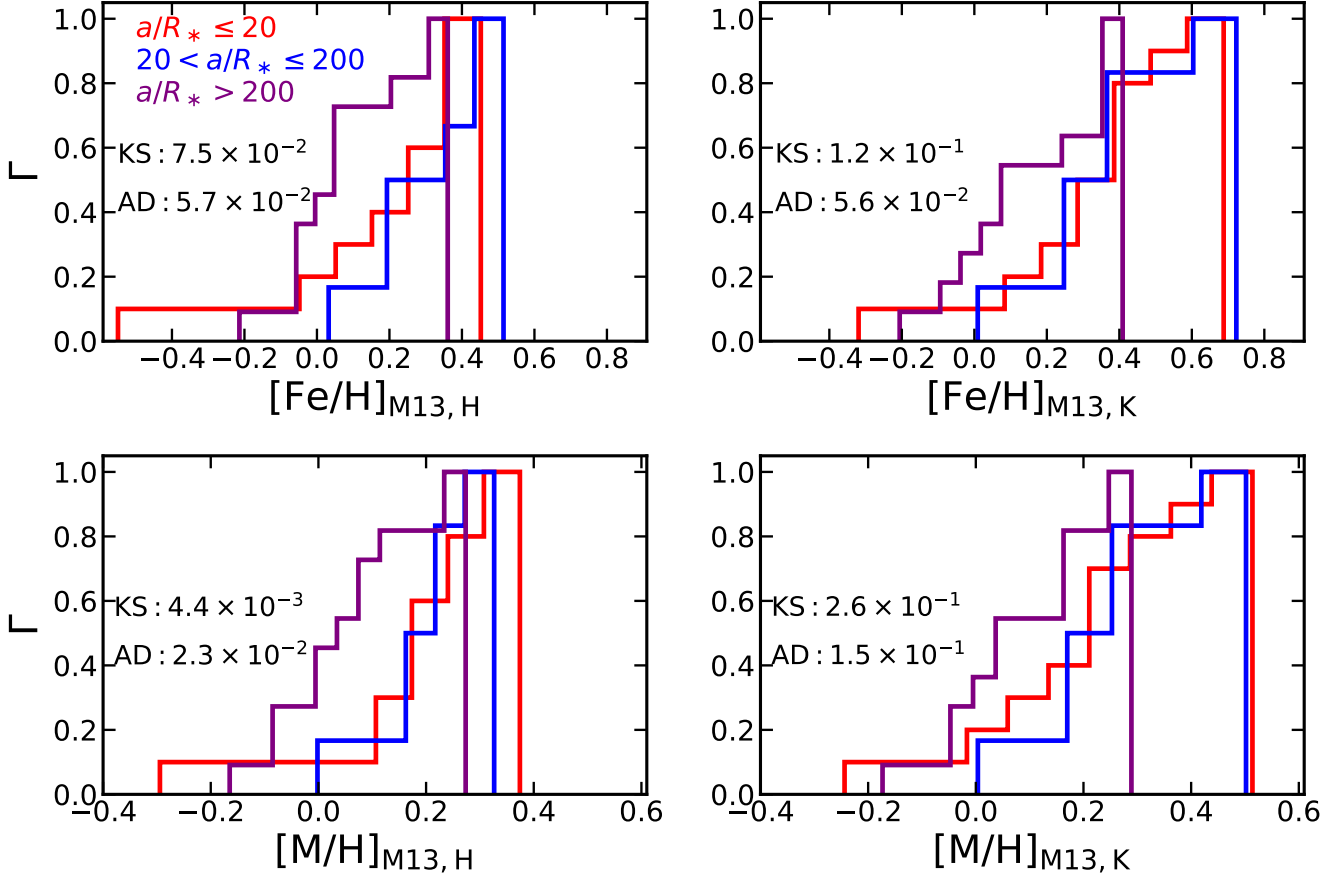


Figure 6. The cumulative [Fe/H] (top) and [M/H] (bottom) distributions from two bands of M dwarfs hosting giant planets located in three different scaled semi-major axis bins: $a/R_* \leq 20$, $20 < a/R_* \leq 200$ and $a/R_* > 200$. The outer cold Jupiters with $a/R_* > 200$ tend to show a weaker preference for metallicity compared with the inner hot Jupiters with $a/R_* \leq 20$. The numbers listed on the left of each panel are the p -values of the K-S and A-D tests between the HJ (red) and CJ (purple) populations.

We thank the anonymous referees and editors for their comments that improved the quality of this publication. We thank Steven Giacalone and Emma Turtelboom for useful discussions. This work is supported by the National Science Foundation of China (Grant No. 12133005). T. G. acknowledges the Tsinghua Astrophysics High-Performance Computing platform at Tsinghua University for providing computational and data storage resources that have contributed to the research results reported within this manuscript. This work is based on data obtained with the NASA Infrared Tele-

scope Facility, which is operated by the University of Hawaii. This research has made use of the NASA Exoplanet Archive, which is operated by the California Institute of Technology, under contract with the National Aeronautics and Space Administration under the Exoplanet Exploration Program.

Facilities: IRTF/SpeX (Rayner et al. 2003)

Software: metal (Mann et al. 2013), SpeXtool (Cushing et al. 2004), SPLAT (Burgasser & Splat Development Team 2017)

APPENDIX

A. RESULTS OF OVERALL METALLICITY [M/H]

We rerun the analysis in Section 5 for all [M/H] measurements. The results are listed in Figure 9 and Table 6. We find that the behavior of [M/H] is similar to those using [Fe/H].

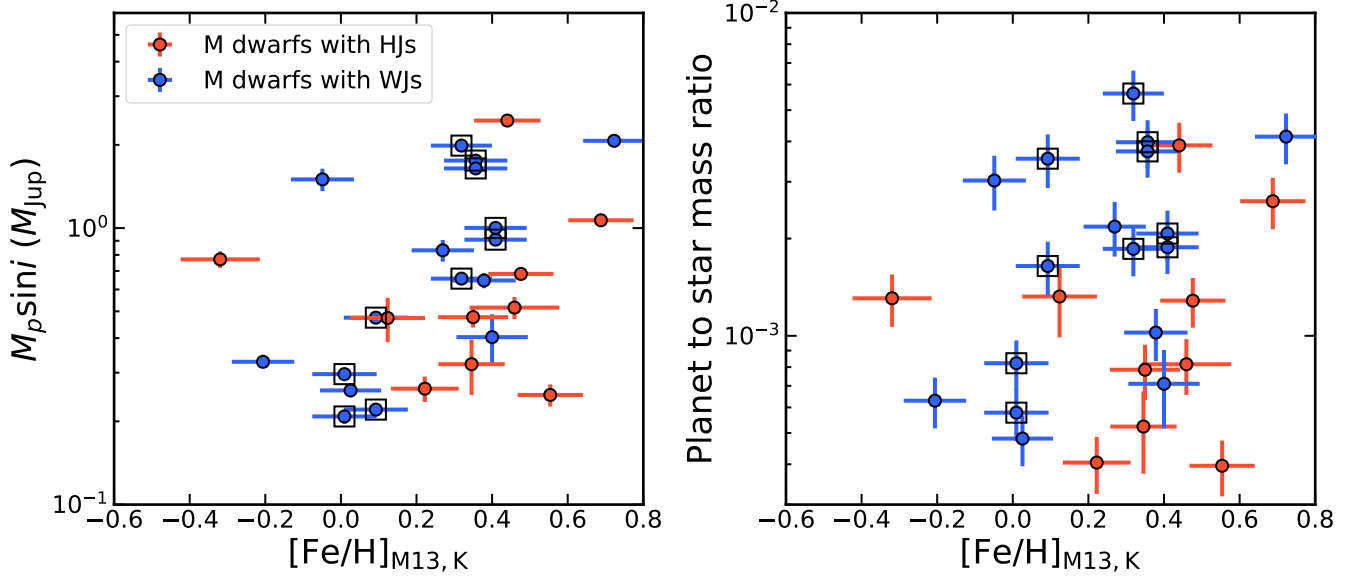


Figure 7. *Left panel:* Refined planet mass versus host metallicity $[\text{Fe}/\text{H}]_{\text{M13,K}}$. The red and blue dots are giant planets with $a/R_* \leq 20$ and $a/R_* > 20$. Five multi-giant planet systems are marked with black boxes. *Right panel:* Similar to the left but for mass ratio.

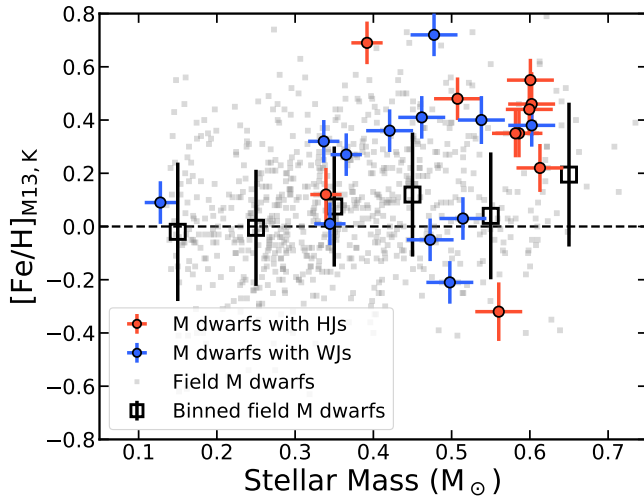


Figure 8. The iron abundance $[\text{Fe}/\text{H}]_{\text{M13,K}}$ vs. stellar mass of 22 M dwarfs with HJs (red) and WJs (blue) in our planet sample. The background grey dots and black squares represent the field M dwarfs and their binned results (binning size= $0.1 M_\odot$) where the uncertainties are the standard deviations in each stellar mass bin.

B. PLANET MASS, SCALED SEMI-MAJOR AXIS AND EQUILIBRIUM TEMPERATURE DISTRIBUTION OF THE GIANT PLANET SAMPLE

In Figure 10, we show the planet mass, scaled semi-major axis and equilibrium temperature distributions of our giant planet sample. We divide the full group into three categories based on their scaled semi-major axis: hot Jupiters ($a/R_* \leq 20$), warm Jupiters ($20 < a/R_* \leq 200$) and cold Jupiters ($a/R_* > 200$). Such a designation is only applied when exploring the stellar metallicity difference between the hot Jupiter and cold Jupiter group (see Section 5.2).

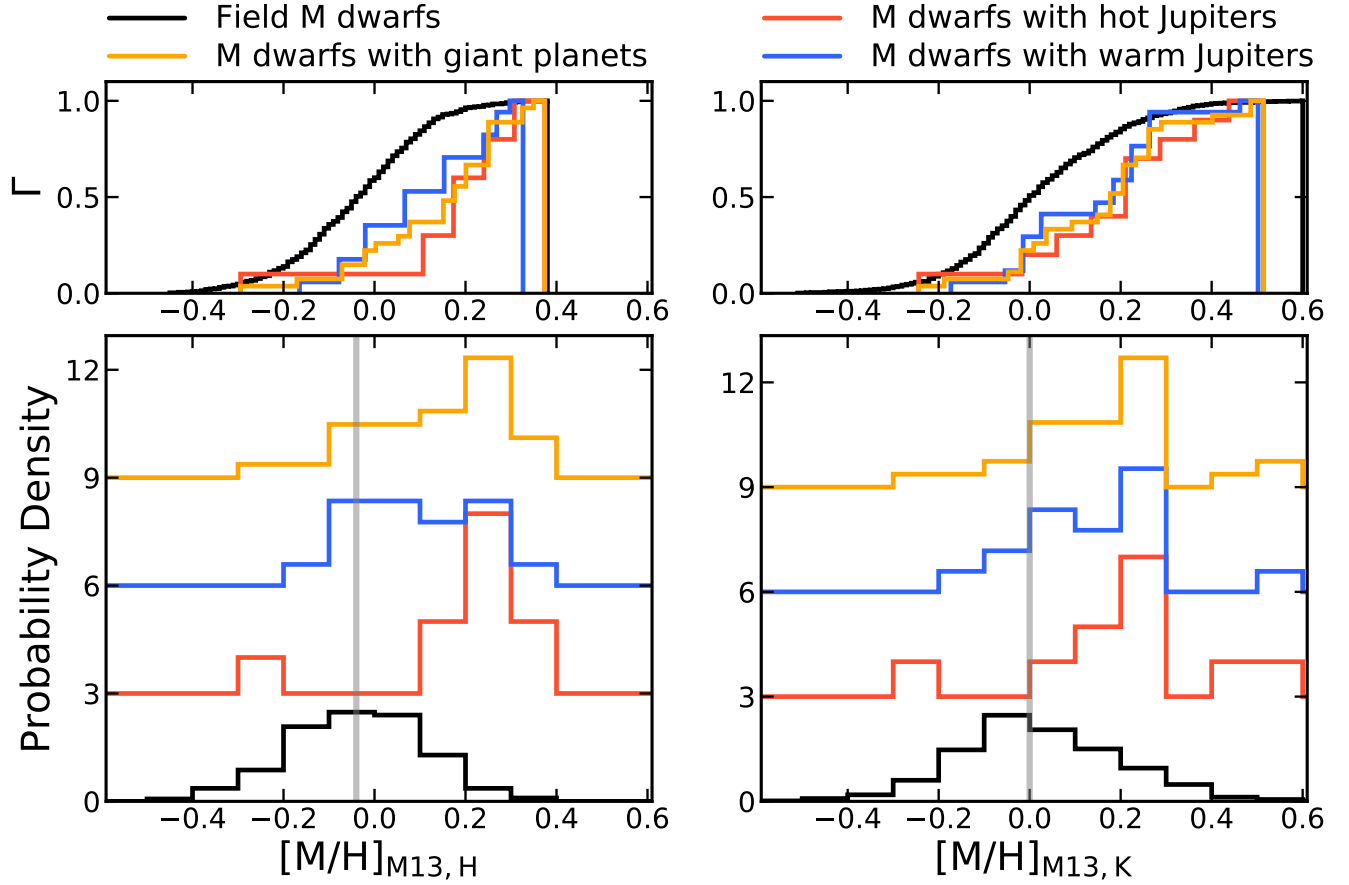


Figure 9. Same as Figure 5 but for $[M/H]_{M13,H}$ and $[M/H]_{M13,K}$. The vertical grey line in each panel marks the median $[M/H]$ of the field M dwarf sample, -0.04 and 0.0 dex. The results are similar to those using $[Fe/H]$.

Table 6. Same as Table 5 but for $[M/H]_{M13,H}$ and $[M/H]_{M13,K}$. The results are similar to those using $[Fe/H]$.

$[M/H]_{M13,H}$	Field M	M + HJ	M + WJ	M + HJ or WJ
Field M	...	9.9×10^{-7} (99.2%)	5.3×10^{-5} (81.5%)	9.9×10^{-7} (100%)
M + HJ	5.1×10^{-8} (93.9%)	...	1.0×10^{-1} (0.7%)	...
M + WJ	5.0×10^{-3} (44.7%)	6.7×10^{-2} (0.9%)
M + HJ or WJ	3.6×10^{-8} (99.6%)
$[M/H]_{M13,K}$	Field M	M + HJ	M + WJ	M + HJ or WJ
Field M	...	1.1×10^{-3} (50.9%)	2.8×10^{-3} (25.0%)	1.5×10^{-5} (98.3%)
M + HJ	3.4×10^{-3} (30.9%)	...	5.6×10^{-1} (0%)	...
M + WJ	6.6×10^{-3} (13.3%)	7.6×10^{-1} (0%)
M + HJ or WJ	4.0×10^{-5} (85.7%)

Adibekyan, V. 2019, *Geosciences*, 9, 105,
doi: [10.3390/geosciences9030105](https://doi.org/10.3390/geosciences9030105)

Akeson, R. L., Chen, X., Ciardi, D., et al. 2013, *PASP*, 125,
989, doi: [10.1086/672273](https://doi.org/10.1086/672273)

Anglada-Escudé, G., Boss, A. P., Weinberger, A. J., et al.
2012, *ApJ*, 746, 37, doi: [10.1088/0004-637X/746/1/37](https://doi.org/10.1088/0004-637X/746/1/37)

Apps, K., Clubb, K. I., Fischer, D. A., et al. 2010, *PASP*,
122, 156, doi: [10.1086/651058](https://doi.org/10.1086/651058)

Bayliss, D., Gillen, E., Eig Müller, P., et al. 2018, *MNRAS*,
475, 4467, doi: [10.1093/mnras/stx2778](https://doi.org/10.1093/mnras/stx2778)

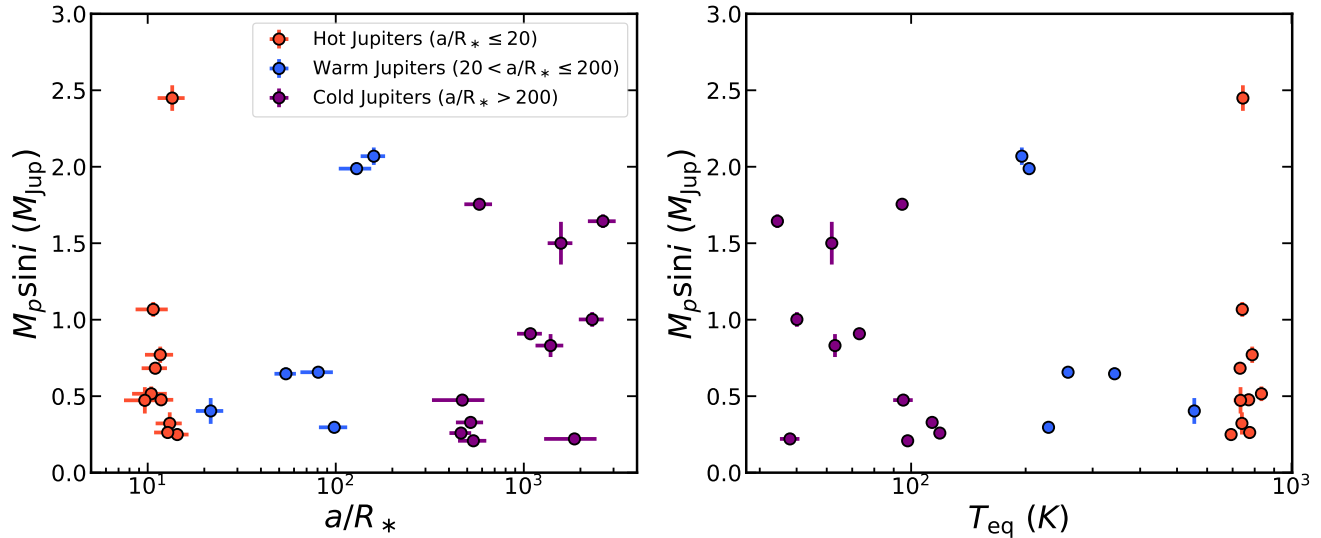


Figure 10. *Left panel:* The planet mass and scaled semi-major axis distribution of our M dwarf giant planet sample. Different colors represent planets with scaled semi-major axis belonging to different ranges (see Section 5.2 for details). *Right panel:* Similar to the left but for equilibrium temperature.

Bello-García, A., Passegger, V. M., Ordieres-Meré, J., et al. 2023, *A&A*, 673, A105,

doi: [10.1051/0004-6361/202243934](https://doi.org/10.1051/0004-6361/202243934)

Bonfils, X., Delfosse, X., Udry, S., et al. 2013, *A&A*, 549, A109, doi: [10.1051/0004-6361/201014704](https://doi.org/10.1051/0004-6361/201014704)

Bonomo, A. S., Desidera, S., Benatti, S., et al. 2017, *A&A*, 602, A107, doi: [10.1051/0004-6361/201629882](https://doi.org/10.1051/0004-6361/201629882)

Borucki, W. J., Koch, D., Basri, G., et al. 2010, *Science*, 327, 977, doi: [10.1126/science.1185402](https://doi.org/10.1126/science.1185402)

Boss, A. P. 2002, *ApJL*, 567, L149, doi: [10.1086/340108](https://doi.org/10.1086/340108)

—, 2006, *ApJ*, 643, 501, doi: [10.1086/501522](https://doi.org/10.1086/501522)

Bryant, E. M., Bayliss, D., & Van Eylen, V. 2023, *MNRAS*, doi: [10.1093/mnras/stad626](https://doi.org/10.1093/mnras/stad626)

Bryant, E. M., Bayliss, D., Hartman, J. D., et al. 2024, *MNRAS*, 533, 3893, doi: [10.1093/mnras/stae2034](https://doi.org/10.1093/mnras/stae2034)

Burgasser, A. J., & Splat Development Team. 2017, in *Astronomical Society of India Conference Series*, Vol. 14, *Astronomical Society of India Conference Series*, 7–12, doi: [10.48550/arXiv.1707.00062](https://doi.org/10.48550/arXiv.1707.00062)

Burn, R., Schlecker, M., Mordasini, C., et al. 2021, *A&A*, 656, A72, doi: [10.1051/0004-6361/202140390](https://doi.org/10.1051/0004-6361/202140390)

Butler, R. P., Johnson, J. A., Marcy, G. W., et al. 2006, *PASP*, 118, 1685, doi: [10.1086/510500](https://doi.org/10.1086/510500)

Cañas, C. I., Stefansson, G., Kanodia, S., et al. 2020, *AJ*, 160, 147, doi: [10.3847/1538-3881/abac67](https://doi.org/10.3847/1538-3881/abac67)

Cañas, C. I., Kanodia, S., Bender, C. F., et al. 2022, *AJ*, 164, 50, doi: [10.3847/1538-3881/ac7804](https://doi.org/10.3847/1538-3881/ac7804)

Correia, A. C. M., Couetdic, J., Laskar, J., et al. 2010, *A&A*, 511, A21, doi: [10.1051/0004-6361/200912700](https://doi.org/10.1051/0004-6361/200912700)

Cushing, M. C., Rayner, J. T., & Vacca, W. D. 2005, *ApJ*, 623, 1115, doi: [10.1086/428040](https://doi.org/10.1086/428040)

Cushing, M. C., Vacca, W. D., & Rayner, J. T. 2004, *PASP*, 116, 362, doi: [10.1086/382907](https://doi.org/10.1086/382907)

Cutri, R. M., Skrutskie, M. F., van Dyk, S., et al. 2003, *2MASS All Sky Catalog of point sources*.

Delamer, M., Kanodia, S., Cañas, C. I., et al. 2024, *ApJL*, 962, L22, doi: [10.3847/2041-8213/ad1a19](https://doi.org/10.3847/2041-8213/ad1a19)

Dressing, C. D., Hardegree-Ullman, K., Schlieder, J. E., et al. 2019, *AJ*, 158, 87, doi: [10.3847/1538-3881/ab2895](https://doi.org/10.3847/1538-3881/ab2895)

Endl, M., Robertson, P., Cochran, W. D., et al. 2022, *AJ*, 164, 238, doi: [10.3847/1538-3881/ac8e05](https://doi.org/10.3847/1538-3881/ac8e05)

Fischer, D. A., & Valenti, J. 2005, *ApJ*, 622, 1102, doi: [10.1086/428383](https://doi.org/10.1086/428383)

Gaia Collaboration, Vallenari, A., Brown, A. G. A., et al. 2023, *A&A*, 674, A1, doi: [10.1051/0004-6361/202243940](https://doi.org/10.1051/0004-6361/202243940)

Gaidos, E., & Mann, A. W. 2014, *ApJ*, 791, 54, doi: [10.1088/0004-637X/791/1/54](https://doi.org/10.1088/0004-637X/791/1/54)

Gaidos, E., Mann, A. W., Lépine, S., et al. 2014, *MNRAS*, 443, 2561, doi: [10.1093/mnras/stu1313](https://doi.org/10.1093/mnras/stu1313)

Gan, T., Lin, Z., Wang, S. X., et al. 2022, *MNRAS*, 511, 83, doi: [10.1093/mnras/stab3708](https://doi.org/10.1093/mnras/stab3708)

Gan, T., Wang, S. X., Wang, S., et al. 2023a, *AJ*, 165, 17, doi: [10.3847/1538-3881/ac9b12](https://doi.org/10.3847/1538-3881/ac9b12)

Gan, T., Cadieux, C., Jahandar, F., et al. 2023b, *AJ*, 166, 165, doi: [10.3847/1538-3881/acf56d](https://doi.org/10.3847/1538-3881/acf56d)

Gonzalez, G. 1997, *MNRAS*, 285, 403, doi: [10.1093/mnras/285.2.403](https://doi.org/10.1093/mnras/285.2.403)

Gore, R., Giacalone, S., Dressing, C. D., et al. 2024, *ApJS*, 271, 48, doi: [10.3847/1538-4365/ad2c0c](https://doi.org/10.3847/1538-4365/ad2c0c)

Haghighipour, N., Vogt, S. S., Butler, R. P., et al. 2010, *ApJ*, 715, 271, doi: [10.1088/0004-637X/715/1/271](https://doi.org/10.1088/0004-637X/715/1/271)

- Han, T., Robertson, P., Kanodia, S., et al. 2024, *AJ*, 167, 4, doi: [10.3847/1538-3881/ad09c2](https://doi.org/10.3847/1538-3881/ad09c2)
- Hartman, J. D., Bayliss, D., Brahm, R., et al. 2015, *AJ*, 149, 166, doi: [10.1088/0004-6256/149/5/166](https://doi.org/10.1088/0004-6256/149/5/166)
- Hartman, J. D., Bakos, G. Á., Csubry, Z., et al. 2023, *AJ*, 166, 163, doi: [10.3847/1538-3881/acf56e](https://doi.org/10.3847/1538-3881/acf56e)
- Hartman, J. D., Bayliss, D., Brahm, R., et al. 2024, *AJ*, 168, 202, doi: [10.3847/1538-3881/ad6f07](https://doi.org/10.3847/1538-3881/ad6f07)
- Henden, A. A., Templeton, M., Terrell, D., et al. 2016, *VizieR Online Data Catalog*, II/336
- Henry, T. J., Jao, W.-C., Subasavage, J. P., et al. 2006, *AJ*, 132, 2360, doi: [10.1086/508233](https://doi.org/10.1086/508233)
- Hodges, J. L. 1958, *Arkiv för Matematik*, 3, 469.
<https://api.semanticscholar.org/CorpusID:121451525>
- Hotnisky, A., Kanodia, S., Libby-Roberts, J., et al. 2024, arXiv e-prints, arXiv:2411.08159, doi: [10.48550/arXiv.2411.08159](https://doi.org/10.48550/arXiv.2411.08159)
- Howard, A. W., Johnson, J. A., Marcy, G. W., et al. 2010, *ApJ*, 721, 1467, doi: [10.1088/0004-637X/721/2/1467](https://doi.org/10.1088/0004-637X/721/2/1467)
- Ida, S., & Lin, D. N. C. 2004a, *ApJ*, 616, 567, doi: [10.1086/424830](https://doi.org/10.1086/424830)
- . 2004b, *ApJ*, 604, 388, doi: [10.1086/381724](https://doi.org/10.1086/381724)
- Jahandar, F., Doyon, R., Artigau, É., et al. 2024, *ApJ*, 966, 56, doi: [10.3847/1538-4357/ad3063](https://doi.org/10.3847/1538-4357/ad3063)
- Johnson, J. A., & Apps, K. 2009, *ApJ*, 699, 933, doi: [10.1088/0004-637X/699/2/933](https://doi.org/10.1088/0004-637X/699/2/933)
- Johnson, J. A., Butler, R. P., Marcy, G. W., et al. 2007, *ApJ*, 670, 833, doi: [10.1086/521720](https://doi.org/10.1086/521720)
- Johnson, J. A., Howard, A. W., Marcy, G. W., et al. 2010, *PASP*, 122, 149, doi: [10.1086/651007](https://doi.org/10.1086/651007)
- Johnson, J. A., Gazak, J. Z., Apps, K., et al. 2012, *AJ*, 143, 111, doi: [10.1088/0004-6256/143/5/111](https://doi.org/10.1088/0004-6256/143/5/111)
- Jordán, A., Hartman, J. D., Bayliss, D., et al. 2022, *AJ*, 163, 125, doi: [10.3847/1538-3881/ac4a77](https://doi.org/10.3847/1538-3881/ac4a77)
- Kagetani, T., Narita, N., Kimura, T., et al. 2023, *PASJ*, doi: [10.1093/pasj/psad031](https://doi.org/10.1093/pasj/psad031)
- Kanodia, S., Libby-Roberts, J., Cañas, C. I., et al. 2022, *AJ*, 164, 81, doi: [10.3847/1538-3881/ac7c20](https://doi.org/10.3847/1538-3881/ac7c20)
- Kanodia, S., Mahadevan, S., Libby-Roberts, J., et al. 2023, *AJ*, 165, 120, doi: [10.3847/1538-3881/acabce](https://doi.org/10.3847/1538-3881/acabce)
- Lépine, S., & Gaidos, E. 2011, *AJ*, 142, 138, doi: [10.1088/0004-6256/142/4/138](https://doi.org/10.1088/0004-6256/142/4/138)
- Lépine, S., & Shara, M. M. 2005, *AJ*, 129, 1483, doi: [10.1086/427854](https://doi.org/10.1086/427854)
- Lin, A. S. J., Libby-Roberts, J. E., Alvarado-Montes, J. A., et al. 2023, *AJ*, 166, 90, doi: [10.3847/1538-3881/ace1ef](https://doi.org/10.3847/1538-3881/ace1ef)
- Liu, B., Lambrechts, M., Johansen, A., & Liu, F. 2019, *A&A*, 632, A7, doi: [10.1051/0004-6361/201936309](https://doi.org/10.1051/0004-6361/201936309)
- Lopez-Santiago, J., Martino, L., Míguez, J., & Vázquez, M. A. 2020, *AJ*, 160, 273, doi: [10.3847/1538-3881/abc171](https://doi.org/10.3847/1538-3881/abc171)
- Maldonado, J., Eiroa, C., Villaver, E., Montesinos, B., & Mora, A. 2012, *A&A*, 541, A40, doi: [10.1051/0004-6361/201218800](https://doi.org/10.1051/0004-6361/201218800)
- Maldonado, J., Micela, G., Baratella, M., et al. 2020, *A&A*, 644, A68, doi: [10.1051/0004-6361/202039478](https://doi.org/10.1051/0004-6361/202039478)
- Mann, A. W., Brewer, J. M., Gaidos, E., Lépine, S., & Hilton, E. J. 2013, *AJ*, 145, 52, doi: [10.1088/0004-6256/145/2/52](https://doi.org/10.1088/0004-6256/145/2/52)
- Mann, A. W., Feiden, G. A., Gaidos, E., Boyajian, T., & von Braun, K. 2015, *ApJ*, 804, 64, doi: [10.1088/0004-637X/804/1/64](https://doi.org/10.1088/0004-637X/804/1/64)
- Mann, A. W., Dupuy, T., Kraus, A. L., et al. 2019, *ApJ*, 871, 63, doi: [10.3847/1538-4357/aaf3bc](https://doi.org/10.3847/1538-4357/aaf3bc)
- Marcy, G. W., Butler, R. P., Vogt, S. S., Fischer, D., & Lissauer, J. J. 1998, *ApJL*, 505, L147, doi: [10.1086/311623](https://doi.org/10.1086/311623)
- Marfil, E., Taberner, H. M., Montes, D., et al. 2021, *A&A*, 656, A162, doi: [10.1051/0004-6361/202141980](https://doi.org/10.1051/0004-6361/202141980)
- Mayor, M., & Queloz, D. 1995, *Nature*, 378, 355, doi: [10.1038/378355a0](https://doi.org/10.1038/378355a0)
- Montet, B. T., Crepp, J. R., Johnson, J. A., Howard, A. W., & Marcy, G. W. 2014, *ApJ*, 781, 28, doi: [10.1088/0004-637X/781/1/28](https://doi.org/10.1088/0004-637X/781/1/28)
- Morales, J. C., Mustill, A. J., Ribas, I., et al. 2019, *Science*, 365, 1441, doi: [10.1126/science.aax3198](https://doi.org/10.1126/science.aax3198)
- Mordasini, C., Alibert, Y., Benz, W., & Naef, D. 2008, in *Astronomical Society of the Pacific Conference Series*, Vol. 398, *Extreme Solar Systems*, ed. D. Fischer, F. A. Rasio, S. E. Thorsett, & A. Wolszczan, 235, doi: [10.48550/arXiv.0710.5667](https://doi.org/10.48550/arXiv.0710.5667)
- Narang, M., Manoj, P., Furlan, E., et al. 2018, *AJ*, 156, 221, doi: [10.3847/1538-3881/aae391](https://doi.org/10.3847/1538-3881/aae391)
- Newton, E. R., Charbonneau, D., Irwin, J., et al. 2014, *AJ*, 147, 20, doi: [10.1088/0004-6256/147/1/20](https://doi.org/10.1088/0004-6256/147/1/20)
- Newton, E. R., Charbonneau, D., Irwin, J., & Mann, A. W. 2015, *ApJ*, 800, 85, doi: [10.1088/0004-637X/800/2/85](https://doi.org/10.1088/0004-637X/800/2/85)
- Osborn, A., & Bayliss, D. 2020, *MNRAS*, 491, 4481, doi: [10.1093/mnras/stz3207](https://doi.org/10.1093/mnras/stz3207)
- Parviainen, H., Palle, E., Zapatero-Osorio, M. R., et al. 2021, *A&A*, 645, A16, doi: [10.1051/0004-6361/202038934](https://doi.org/10.1051/0004-6361/202038934)
- Pass, E. K., Winters, J. G., Charbonneau, D., et al. 2023, *AJ*, 166, 11, doi: [10.3847/1538-3881/acd349](https://doi.org/10.3847/1538-3881/acd349)
- Passegger, V. M., Schweitzer, A., Shulyak, D., et al. 2019, *A&A*, 627, A161, doi: [10.1051/0004-6361/201935679](https://doi.org/10.1051/0004-6361/201935679)
- Passegger, V. M., Bello-García, A., Ordieres-Meré, J., et al. 2022, *A&A*, 658, A194, doi: [10.1051/0004-6361/202141920](https://doi.org/10.1051/0004-6361/202141920)
- Petigura, E. A., Marcy, G. W., Winn, J. N., et al. 2018, *AJ*, 155, 89, doi: [10.3847/1538-3881/aaa54c](https://doi.org/10.3847/1538-3881/aaa54c)

- Pinamonti, M., Barbato, D., Sozzetti, A., et al. 2023, *A&A*, 677, A122, doi: [10.1051/0004-6361/202346476](https://doi.org/10.1051/0004-6361/202346476)
- Pollack, J. B., Hubickyj, O., Bodenheimer, P., et al. 1996, *Icarus*, 124, 62, doi: [10.1006/icar.1996.0190](https://doi.org/10.1006/icar.1996.0190)
- Quirrenbach, A., Passegger, V. M., Trifonov, T., et al. 2022, *A&A*, 663, A48, doi: [10.1051/0004-6361/202142915](https://doi.org/10.1051/0004-6361/202142915)
- Rayner, J. T., Cushing, M. C., & Vacca, W. D. 2009, *ApJS*, 185, 289, doi: [10.1088/0067-0049/185/2/289](https://doi.org/10.1088/0067-0049/185/2/289)
- Rayner, J. T., Toomey, D. W., Onaka, P. M., et al. 2003, *PASP*, 115, 362, doi: [10.1086/367745](https://doi.org/10.1086/367745)
- Reyl e, C., Jardine, K., Fouqu e, P., et al. 2021, *A&A*, 650, A201, doi: [10.1051/0004-6361/202140985](https://doi.org/10.1051/0004-6361/202140985)
- Ricker, G. R., Winn, J. N., Vanderspek, R., et al. 2015, *Journal of Astronomical Telescopes, Instruments, and Systems*, 1, 014003, doi: [10.1117/1.JATIS.1.1.014003](https://doi.org/10.1117/1.JATIS.1.1.014003)
- Rivera, E. J., Laughlin, G., Butler, R. P., et al. 2010, *ApJ*, 719, 890, doi: [10.1088/0004-637X/719/1/890](https://doi.org/10.1088/0004-637X/719/1/890)
- Robin, A. C., Reyl e, C., Derri ere, S., & Picaud, S. 2003, *A&A*, 409, 523, doi: [10.1051/0004-6361:20031117](https://doi.org/10.1051/0004-6361:20031117)
- Rojas-Ayala, B., Covey, K. R., Muirhead, P. S., & Lloyd, J. P. 2010, *ApJL*, 720, L113, doi: [10.1088/2041-8205/720/1/L113](https://doi.org/10.1088/2041-8205/720/1/L113)
- . 2012, *ApJ*, 748, 93, doi: [10.1088/0004-637X/748/2/93](https://doi.org/10.1088/0004-637X/748/2/93)
- Rosenthal, L. J., Fulton, B. J., Hirsch, L. A., et al. 2021, *ApJS*, 255, 8, doi: [10.3847/1538-4365/abe23c](https://doi.org/10.3847/1538-4365/abe23c)
- Sabotta, S., Schlecker, M., Chaturvedi, P., et al. 2021, *A&A*, 653, A114, doi: [10.1051/0004-6361/202140968](https://doi.org/10.1051/0004-6361/202140968)
- Santos, N. C., Israelian, G., & Mayor, M. 2004, *A&A*, 415, 1153, doi: [10.1051/0004-6361:20034469](https://doi.org/10.1051/0004-6361:20034469)
- Scholz, F. W., & Stephens, M. A. 1987, *Journal of the American Statistical Association*, 82, 918. <http://www.jstor.org/stable/2288805>
- Skrutskie, M. F., Cutri, R. M., Stiening, R., et al. 2006, *AJ*, 131, 1163, doi: [10.1086/498708](https://doi.org/10.1086/498708)
- Sousa, S. G., Santos, N. C., Israelian, G., Mayor, M., & Udry, S. 2011, *A&A*, 533, A141, doi: [10.1051/0004-6361/201117699](https://doi.org/10.1051/0004-6361/201117699)
- Sozzetti, A. 2023, *A&A*, 670, L17, doi: [10.1051/0004-6361/202245454](https://doi.org/10.1051/0004-6361/202245454)
- Stefansson, G., Mahadevan, S., Winn, J., et al. 2024, arXiv e-prints, arXiv:2410.05654, doi: [10.48550/arXiv.2410.05654](https://doi.org/10.48550/arXiv.2410.05654)
- Terrien, R. C., Mahadevan, S., Bender, C. F., et al. 2012, *ApJL*, 747, L38, doi: [10.1088/2041-8205/747/2/L38](https://doi.org/10.1088/2041-8205/747/2/L38)
- Terrien, R. C., Mahadevan, S., Deshpande, R., & Bender, C. F. 2015, *ApJS*, 220, 16, doi: [10.1088/0067-0049/220/1/16](https://doi.org/10.1088/0067-0049/220/1/16)
- Thorngren, D. P., Fortney, J. J., Murray-Clay, R. A., & Lopez, E. D. 2016, *ApJ*, 831, 64, doi: [10.3847/0004-637X/831/1/64](https://doi.org/10.3847/0004-637X/831/1/64)
- Trifonov, T., K urster, M., Zechmeister, M., et al. 2018, *A&A*, 609, A117, doi: [10.1051/0004-6361/201731442](https://doi.org/10.1051/0004-6361/201731442)
- Veyette, M. J., Muirhead, P. S., Mann, A. W., & Allard, F. 2016, *ApJ*, 828, 95, doi: [10.3847/0004-637X/828/2/95](https://doi.org/10.3847/0004-637X/828/2/95)
- Virtanen, P., Gommers, R., Oliphant, T. E., et al. 2020, *Nature Methods*, 17, 261, doi: [10.1038/s41592-019-0686-2](https://doi.org/10.1038/s41592-019-0686-2)